NASA Contractor Report CR-180864

FUEL-INJECTOR/AIR-SWIRL CHARACTERIZATION

J.B. McVey, J.B. Kennedy and S. Russell

United Technologies Research Center
East Hartford, Connecticut

January 1988

Prepared for
NATIONAL AERONAUTICS AND SPACE ADMINISTRATION
Lewis Research Center
NAS3-24352

NASA Contractor Report CR-180864

FUEL-INJECTOR/AIR-SWIRL CHARACTERIZATION

J.B. McVey, J.B. Kennedy and S. Russell

United Technologies Research Center
East Hartford, Connecticut

January 1988

Prepared for
NATIONAL AERONAUTICS AND SPACE ADMINISTRATION
Lewis Research Center
NAS3-24352

1. Report No.	2. Government Accession No.	3. Recipient's Catalog No.
NASA CR-180864		

4. Title and Subtitle	5. Report Date
Fuel-Injector/Air-Swirl Characterization	January 1988
	6. Performing Organization Code
7. Author(s)	8. Performing Organization Report No.
J. B. McVey, J. B. Kennedy, S. Russell	
9. Performing Organization Name and Address	10. Work Unit No.
United Technologies Research Center Silver Lane East Hartford, CT 06108	11. Contract or Grant No. NAS3-24352
12. Sponsoring Agency Name and Address	13. Type of Report and Period Covered Contractor Report
National Aeronautics and Space Administration Washington, D.C. 20546	14. Sponsoring Agency Code

15. Supplementary Notes

Final Report. Project Manager, Daniel Bulzan
Internal Fluid Mechanics Division, NASA Lewis Research Center
Cleveland, OH 44135

16. Abstract

Experimental data on the characteristics of the spray produced by a gas-turbine engine airblast fuel injector are reported. The data acquired include the mass-flux distribution measured by use of a high-resolution spray patternator; the gas-phase velocity field measured by use of a two-component laser Doppler velocimeter, and the liquid droplet size and velocity distributions measured by use of a single-component phase-Doppler anemometer. The data are intended for use in assessments of two-phase flow computational methods as applied to combustor design procedures.

17. Key Words (Suggested by Author(s))	18. Distribution Statement
Spray modeling, laser diagnostics, fuel injectors	Unclassified

19. Security Classif. (of this report)	20. Security Classif. (of this page)	21. No. of Pages	22. Price*
Unclassified	Unclassified	54	

* For sale by the National Technical Information Service, Springfield, Virginia 22161

TABLE OF CONTENTS

FUEL-INJECTOR/AIR-SWIRL CHARACTERIZATION

John B. McVey, Jan B. Kennedy, and Sid Russell

United Technologies Research Center

SUMMARY

An experimental program was conducted to obtain information on the characteristics of the spray produced by a gas turbine fuel injector. The objective of the study was to obtain spatially-resolved information on the spray flow field under the conditions of high-flow, high velocity and high swirl which are characteristic of actual engine injector operation. Sufficient data was collected such that an evaluation can be made of the effectiveness of currently-available computational fluid dynamic calculation procedures for predicting spray behavior.

A single airblast nozzle operating with water as the injectant was employed. Measurements were made in unconfined flow at atmospheric pressure at a flow rate of approximately 70 kg/hr and with a characteristic gas phase velocity of 125 mps. Measurements were performed using a high-resolution spray patternator, a two-component laser velocimeter, and a single-component phase Doppler anemometer. Diametral traverses were performed at measurement stations ranging from 0.11 to 10.56 cm downstream of the injector.

Data reported include gas-phase axial velocity, liquid-phase axial velocity, droplet size, and liquid mass flux. Also reported for the condition of gas-flow-only are the first moment (fluctuating component) of the axial velocity and the mean and fluctuating components of tangential and radial velocity.

INTRODUCTION

The achievement of a predictable and satisfactory distribution of finely atomized fuel is of importance to the design of well-performing gas turbine engine combustion chambers. The development of non-intrusive laser diagnostics offers the possibility of acquiring detailed point-resolved data on the gas and liquid-phase flow fields and data giving the droplet size distribution produced by fuel injectors. The availability of such data will aid in the identification of analytic design procedures appropriate to the specification of injector/burner configurations (number of injectors, primary combustion air entrance port location, etc.) as well as the specification of injector/swirler design details (swirler vane angle, filmer diameter, etc.). These analytic design procedures will be based on computational fluid mechanic analyses capable of treating two- and three-dimensional, two-phase, reacting flows. Numerous computer codes are under development for this application. The sophistication required for the treatment of the two-phase flow processes will have a major influence on the complexity of the analysis required and, therefore, on the extent of labor and computer resources needed to exercise the design procedures. The objective of this study is to provide experimental data on the behavior of an injector/swirler-produced flow for a configuration and a condition which more closely approximate those in an engine combustor than do currently available data. These data will be useful in the evaluation of the various analytical treatments of the fuel injection problem.

For this study, it is required that point-resolved (spatially-precise) information on the flow characteristics of both the gas phase and liquid phase be obtained in a representative spray. The work performed to date along these lines includes: (1) efforts carried out in order to prove the capability of new instrumentation techniques; (2) efforts to examine simplified, idealized flows under tightly controlled conditions in order to provide benchmark data for the assessment of the physical models to be employed in computational procedures; and (3) efforts to document the behavior of fuel injectors.

The earliest attempts to apply laser diagnostics to the documentation of a two-phase velocity field were performed using standard laser Doppler velocimetry (LDV). Signal amplitude alone was used to distinguish between the doppler signals produced by the micron-sized seed particles used to track the gas motion and the much larger signals produced by the droplets. This technique was generally found to be unsatisfactory because the signals generated by droplets grazing the sampling volume were of the same amplitude as those generated by seed particles fully within the sample volume. The contamination of the seed-produced signals by the spurious droplet-produced signals is sometimes referred to as "signal cross-talk". This problem was addressed by Modarress et al (Ref. 1-3) who used amplitude-discrimination techniques to identify and reject the spurious signals. The flow studied was that of a fully-developed, turbulent, two-phase flow (air and glass microspheres) issuing from a 20mm circular tube. Mean and rms velocities of the gas and solid phases were reported for flows having peak velocities of approximately 10 m/s and mass loadings (ratio of solids to gas) of 0.3 and 0.9. Spherical glass beads with diameters of 200 and 50 micron diameter were employed. (Use of monodisperse particles of known size is a useful means of simplifying the general problem and eliminating the need for the modeler to assign a particle size distribution to be used in initializing the problem.)

A similar study was performed by Faeth and co-workers (Refs. 4 and 5), who studied a two-phase jet that issued from a 10.9 mm dia. tube into a quiescent environment. An LDV system employing amplitude discrimination techniques and the use of a high seed rate to minimize signal cross-talk were utilized. Flow velocities of approximately 30 m/s, loading ratios of 0.2 and 0.7, and particle (sand) sizes of from 80 to 200 microns were employed.

The two-phase jet flow problem was further documented by Mostafa et al (Ref. 6) using more-recently-developed instrumentation. Flows issuing from a 25.3mm tube at velocities on the order of 5 m/s with spherical glass beads 100-110 microns in diameter were studied in detail. Mass loading ratios of 0.2 and 1.0 were employed. A two-component phase-Doppler anemometer (PDA) was employed in these tests. The mean and rms velocities of the gas and particles, and the gas-phase turbulent shear stress were measured. The phase-Doppler technique (discussed below) permits determination of both the particle size and velocity; the instrument specifically eliminates the signal cross-talk problem by its capability to discriminate particle size.

Information on the effect of swirl on a two-phase jet flow was supplied by Bulzan et al (Ref. 7) who studied swirling jet containing 39 micron glass beads at loading ratios from 0 to 0.33. The swirl levels were relatively low such that vortex breakdown was prevented (swirl number of 0.3); the characteristic velocity was 15 m/sec. Mean and fluctuating velocity measurements of the axial and tangential velocity components are reported for both gas and solid phases. Conventional laser velocimetry, phase-Doppler anemometry and isokinetic sampling techniques were employed.

Recent work on actual sprays includes the work of Solomon et al (Refs. 8, 9, 10) who reported measurements of the velocity field in the dilute region of a spray produced by an airblast nozzle. A conventional LDV system was used to measure mean and fluctuating velocity components, including Reynolds stress distributions. Signal cross-talk was surpressed by utilizing high gas-phase seed rates. Path-averaged droplet sizes were measured using a Malvern 3300 droplet analyzer while local values of mean droplet size were obtained using slide-impact techniques. Injectant flow rates up to 5 kg/hr, loading ratios up to 6.5 and flow velocities up to 150 m/s were employed.

During the development of the phase-Doppler anemometer, Bachalo and co-workers performed measurements on the characteristics of sprays produced by pressure-atomizing swirl nozzles. In one case (Ref. 11), the flows were dominated by the liquid phase with only a small quantity of air used to purge the system. Liquid flow rates to 132 kg/hr, droplet size ranges from 40 to 350 microns and velocities to 20 m/sec were recorded. Both axial and radial components of droplet velocity were reported along with the spatially-resolved droplet size such that particle trajectories could be studied.

These studies were then extended to include the effects of an external, non-swirling gas flow on the spray trajectory (Ref. 12). Water, at a flow rate of 11.4 kg/hr, was discharged into co-flowing airstreams which had velocities from 12 to 30 m/sec. Measurements of the radial distribution of mean axial velocity, mean radial velocity and SMD were reported for five downstream measurement locations. Number density measurements were reported

and indicated that the nozzle produced a center-peaked mass flux distribution.

Kraemer and Bachalo (Ref. 13) applied the phase-Doppler instrument to a high-flow (64 kg/hr) nozzle which employed a low-flow pressure-atomizing primary flow passage and a high-flow air-blast secondary circuit. Limited information on the radial droplet size variation (150-700 microns) was obtained in 15 m/s flows at a station 5 cm downstream of the nozzle exit.

The characteristics of airblast nozzles have been reported in detail by Samuelsen (Refs. 14-16). Laser interferrometric techniques and diffraction techniques were used in early work on small nozzles (Ref. 14). Later efforts employed a phase-Doppler anemometer to measure the radial distribution of droplet size and mean axial velocity at a given axial station for a series of airblast nozzles (Ref. 15) and to examine the number density and azimuthal velocity distribution of combusting sprays confined within a quartz combustor (Ref. 16). Nozzles operating at flow rates of 3-8 kg/hr developing flow velocities on the order of 10 m/sec were employed.

Chigier and co-workers (Ref. 17) report an investigation of a non-swirling air-assist atomizer in which the PDA instrument was used to provide limited information on the radial distribution of mean and fluctuating axial droplet velocity, droplet size and spray volume flux and number density. Water flow rates of 7 and 21 kg/hr, loading ratios of 0.7 and 2.3, and characteristic velocities of 30 m/s were employed.

The objective of the present study is to obtain information on the operation of a large-scale airblast nozzle under isothermal conditions in which a strong interaction of a swirling airstream with a liquid spray occurs--the intent is to closely simulate the fluid behavior in a combustor. The conditions are more demanding than previous studies relative to the capabilities of the instrumentation; of particular impact was the combination of high liquid flow rate, high flow velocity and high swirl. The approach was to apply three instrumentation techniques to characterize the fuel spray: a high resolution patternator for establishing the spray mass flux distribution; a two-component LDV for documenting the three components of gas flow velocity produced by the injector swirlers in the absence of the spray; and a single-component PDA for obtaining information on the spatial distribution of mean droplet size and of the axial component of velocity of both phases.

The information obtained on the behavior of sprays under these conditions should provide a basis for determining which processes must be included in analyses in order to generate an adequate description of fuel distribution in engine combustors. The major effect to be considered is, of course, the relative motion between the two phases and the effect of the resulting particle drag on the spray trajectory. Higher-order effects which are currently under study include: the influence of the gas-phase turbulence on the trajectory of the droplets (Ref. 18); the suppression of the gas-phase turbulence by the droplets (Ref. 19); the droplet-droplet interactions which can result in coalescence or droplet breakup (Refs. 20, 21) and modification of the droplet drag laws due to the influence of neighboring droplets (Ref. 22). The various methods of analysis have been thoroughly reviewed in the literature (e.g., Ref. 23).

TEST APPARATUS AND INSTRUMENTATION

Fuel Nozzle

An airblast fuel nozzle (Fig. 1) was employed in this study. This atomizer concept is well established (Ref. 24) and is employed in current high-thrust gas turbine engines. Fuel is supplied at low pressure to a filming surface on both sides of which flows high-velocity swirling air--the shearing action of the airstreams act to atomize the fuel. This nozzle was sized as a 375 kg/hr unit. The particular nozzle used can be easily disassembled such that the effect of component design changes on the spray characteristics can be readily evaluated (Ref. 25).

The configuration employed (Fig. 2) embodies inner and outer clockwise (when viewed from the upstream direction) air-swirlers. The final turning angle of the 16 helical vanes of the outer swirler is 40 deg. This swirling flow is turned radially inward by the end cap which imparts a radial-inflow velocity component and which results in a further increase in swirl angle. The flow discharges through a 4mm gap at a mean angle of 62.5 deg relative to the injector axis.

The 14-vane inner swirler employs straight vanes with a turning angle of 45 deg. The resulting annular swirling flow is contracted to a smaller diameter tubular flow, thereby increasing the gas rotational velocity.

The fuel is distributed through a 2mm annular gap. Within this gap is located a blockage ring containing six 7.6 mm wide slots which swirl the flow at an angle of 55 deg. At the discharge end, the swirling flow is turned radially inward and is discharged through a slightly-converging passage having a mean angle of 52.5 deg relative to the injector axis.

The particular combination of components employed was selected on the basis of measured ability to produce spray with a high degree of circumferential uniformity, in addition to the ability to produce a representative radial mass flow distribution and satisfactory atomization.

Installation

All testing was conducted under unconfined, atmospheric pressure conditions at ambient temperature. Water was primarily used as the injectant for the tests, however, Jet-A was also used in the patternator tests.

For the patternator tests, the injector was mounted with the flow axis vertical. For the LDV and PDA measurements, the flow axis was horizontal. Patternation tests conducted previously have determined that, under the high flow conditions employed in these tests, the spray characteristics are independent of gravitational effects.

For the LDV and PDA tests, the injector was mounted in a fixturing device, Figs. 3 and 4, which acted as a plenum for the seeded air supply and which permitted the injector to be rotated about its centerline. This fixture was rigidly attached to the air supply centerline which was adjacent to and

Figure 1. Airblast fuel nozzle.

87 – 10 – 66 – 1

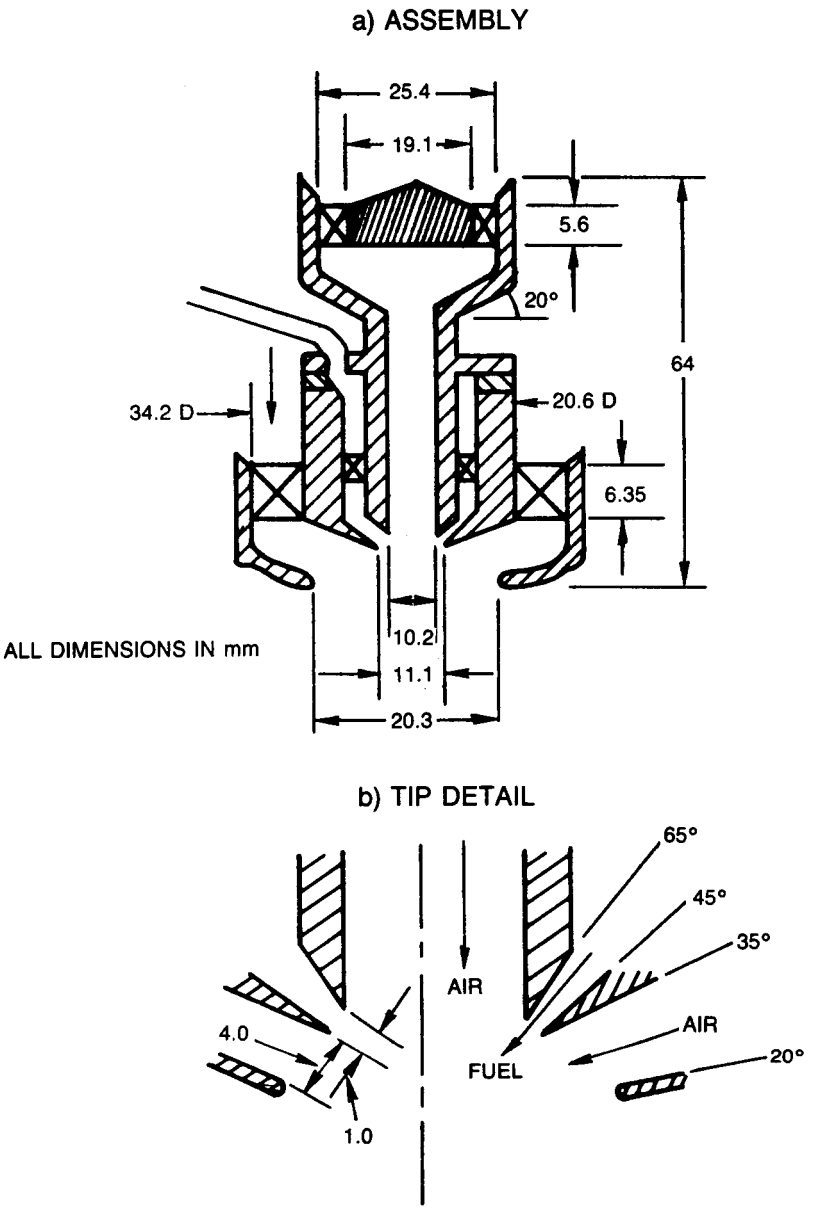

Figure 2. Fuel nozzle dimensions.

87-10-66-2

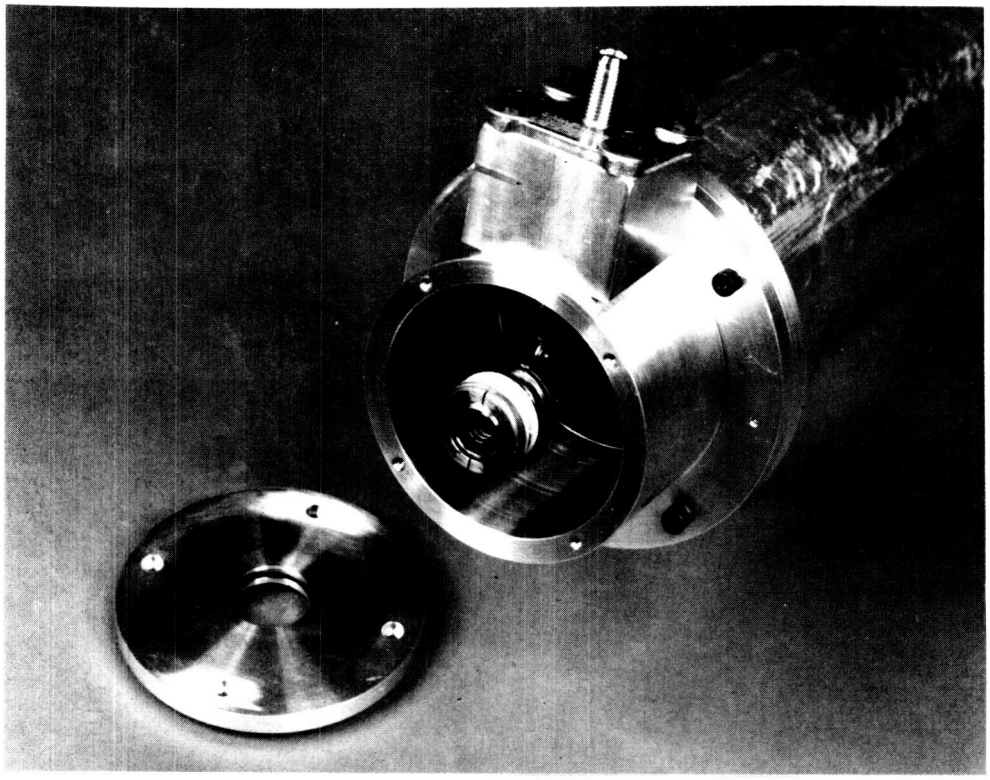

Figure 3. Typical fuel nozzle installation.

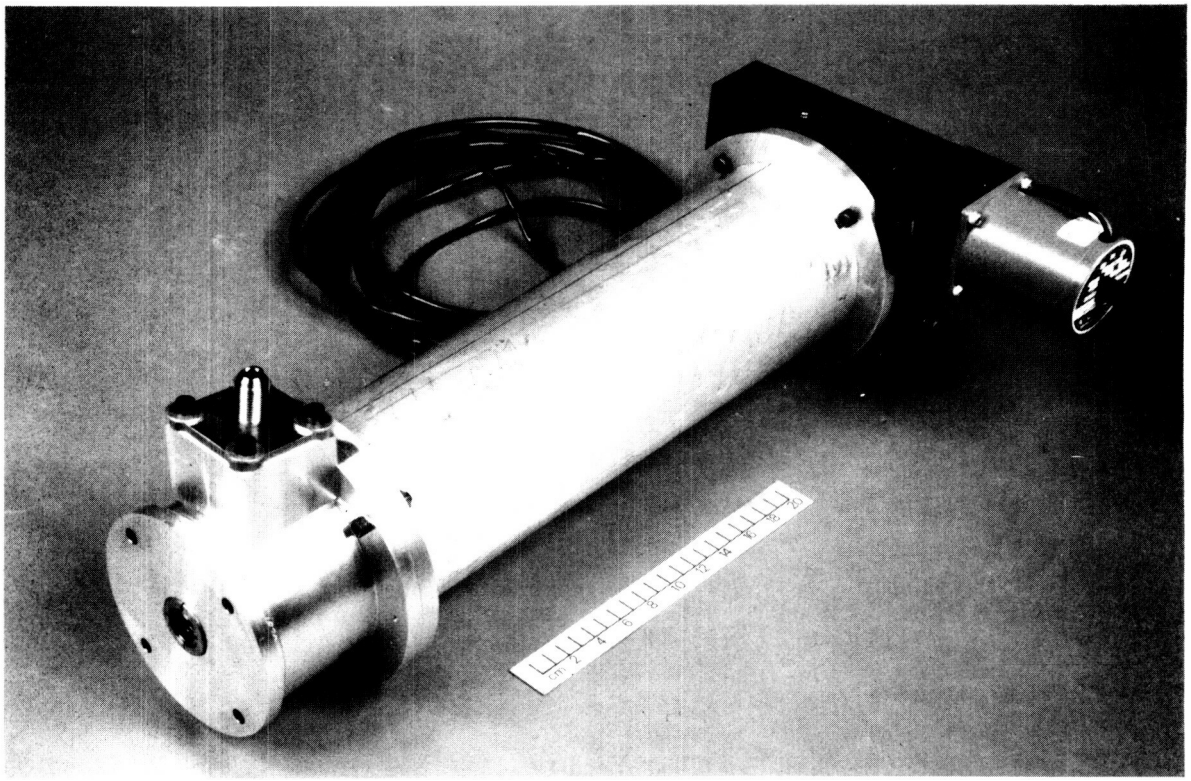

Figure 4. Fuel nozzle airflow characterization test device.

aligned with an optical table on which all the optical instrumentation was mounted (Fig. 5). The air flowing through the injector swirler discharged into the ambient surroundings. At a location approximately 150 cm downstream of the injector, a 46 cm dia. duct, which was under a slight negative pressure produced by the ejector action of a water spray, captured the seeded airflow. The flow velocity induced on the axis of the test region at the farthest downstream measurement station was less than 1 m/s.

A diagram showing the measurement axes and the definitions of the positive velocity vectors is given in Fig. 6. Note that in this figure the flow is viewed from the downstream direction and hence the sense of rotation of the flow is counterclockwise.

Spray Patternator

A high-resolution spray patternator (Ref. 26) was used to establish the circumferential uniformity of the fuel spray. The patternator (Fig. 7) employs extractive probing by use of multiple-point rakes to acquire data on spray mass flux distributions under ambient pressure conditions. Sixty sampling probes with squared, chamfered entrance sections are arranged in linear arrays of 10 units each radiating from the patternator axis. The probes are fixed in space while the fuel nozzle fixturing enclosure is positioned azimuthally using a precision rotation stage. For the experiments conducted in this program, a 5-deg angular increment was employed such that 720 data points were used to construct each mass flux distribution contour map.

The test conditions are established by delivering a metered amount of injectant and by establishing a specified pressure differential between the fixturing enclosure and ambient. The flow rate of air is maintained using a back pressure regulator and a choked venturi. The mass flux at each sampling probe location is determined from the amount of fluid collected per unit time and the probe entrance area. The reported values are the flux values through a plane surface normal to the injector axis (not through a spherical surface).

A Malvern ST1800 Particle Analyzer (Refs. 27 & 28) is used in conjunction with the patternator. This instrument analyzes the distribution of the intensity of light scattered from a laser beam passing through the fuel spray. A measure of the path-averaged spray droplet size distribution is obtained by obtaining a best fit between the measured data and that produced (according to Mie-scattering theory) by a spray having a Rosin-Raemmler drop size distribution. The corresponding path-averaged SMD values are reported.

The range of possible measuring station locations is dictated by the characteristics of the system. At large distances, the conically-shaped spray will not be completely captured by the 10.2 cm dia. probe array. At small distances, probe resolution is lost and the spray density causes excessive beam obscuration which results in biasing of the SMD measurements data (Ref. 29). General practice has been to perform patternation measurements of this nozzle type at a distance of 5.4 cm. A measurement range of from 2.54 to 6.35 cm was used in the program.

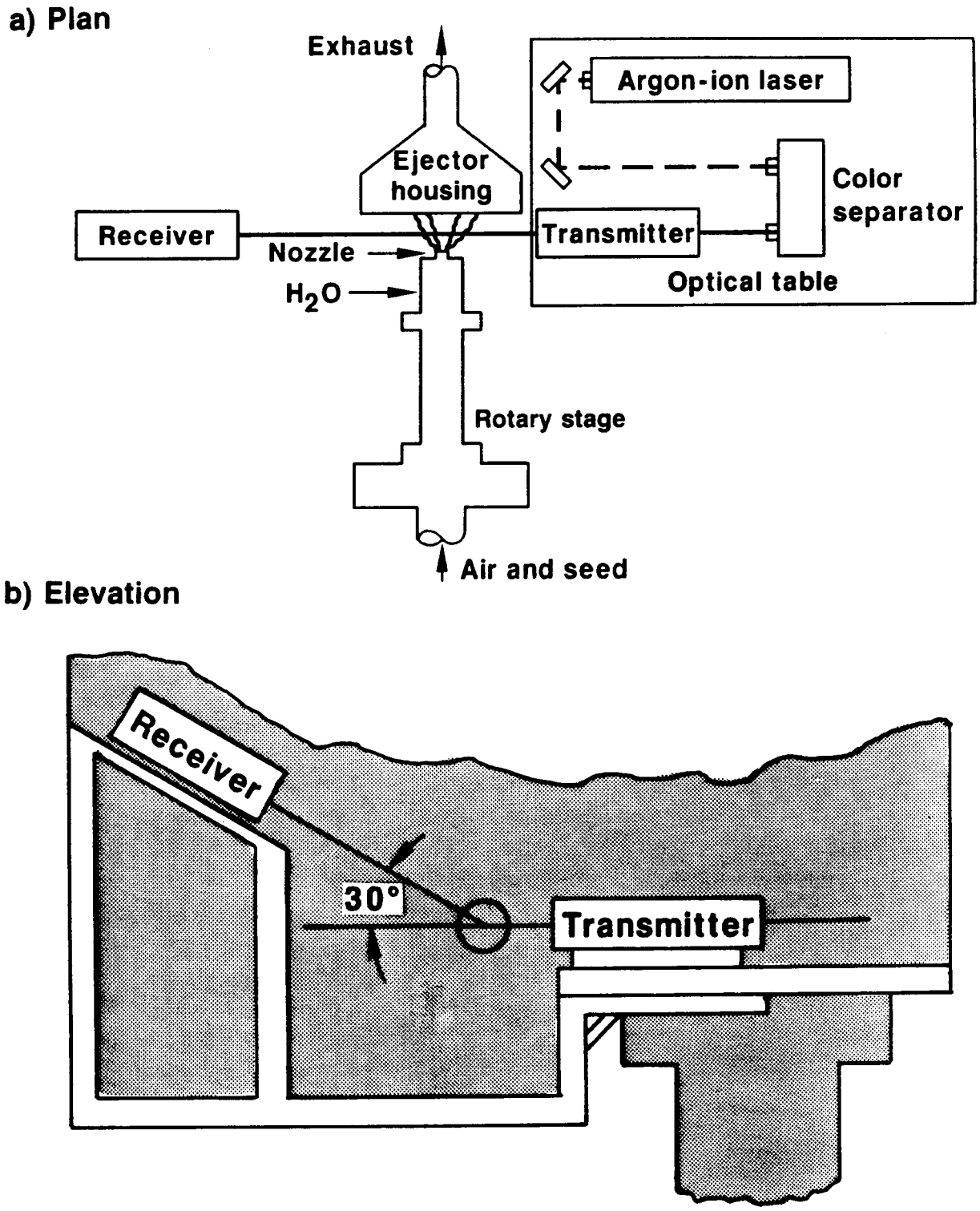

Figure 5 . Laser diagnostics — general arrangement.

ORIGINAL PAGE IS
OF POOR QUALITY

87-10-66-3

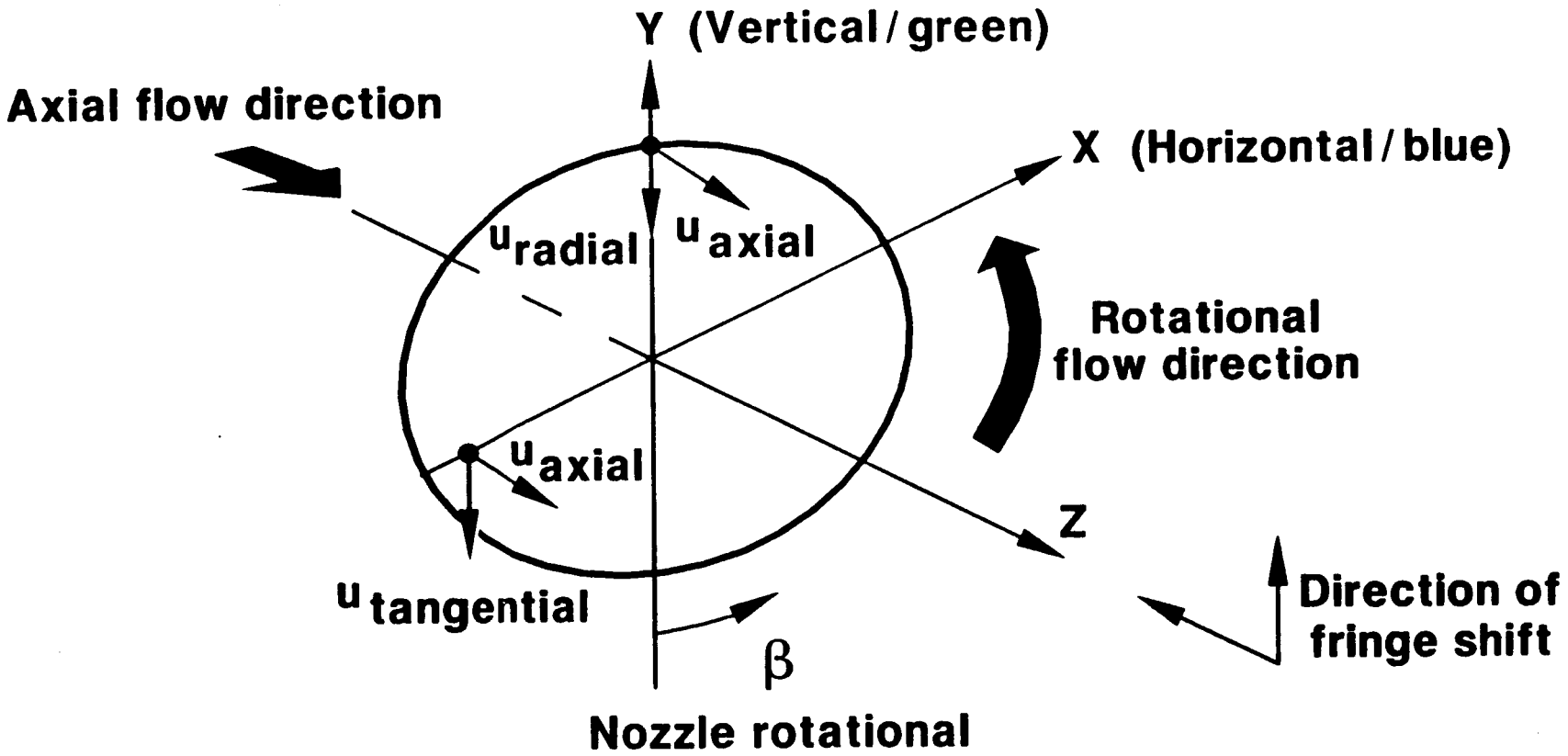

Figure 6. Coordinate and velocity component definition.

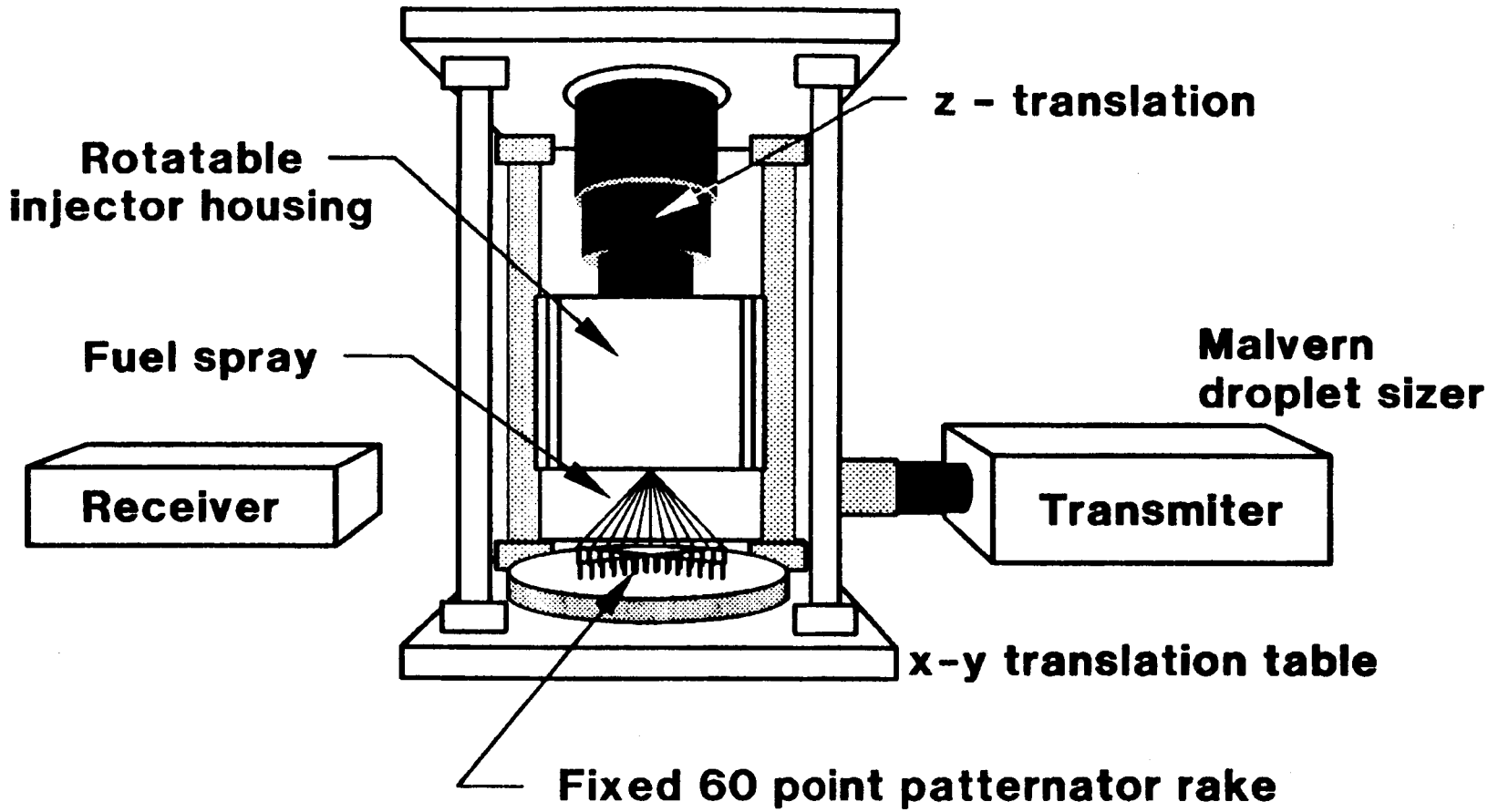

Figure 7. Spray apparatus configuration.

Laser Velocimeter

The velocimeter employed was a standard configuration TSI Model 9100-7, two-channel velocimeter (Fig. 8). An argon-ion laser operating at a power output of two watts was used; frequency shifting by Bragg cells located in both the blue and green incident beams provided the capability for resolving negative velocities. For this program, the velocimeter was operated in the non-coincident data acquisition mode in order to achieve high data rates in the low-seed concentration regions (the requirement for coincident detection of signals from the two channels was not imposed--turbulence cross-correlation data were not obtained). Processor parameter settings were optimized for the particular velocity ranges encountered:

	Blue Channel	Green Channel
Transmitted Beam Plane Orientation	Horizontal	Vertical
Measured Velocity Component	Axial	Tangential/Radial
Velocity Range (mps)	-10 to +70	$\pm$120
Beam Convergence Half-Angle (Deg)	1.68	2.40
Doppler Frequency (mps/mHz)	8.33	6.14
Frequency Offset (mHz)	10	40
Bandpass (mHz)	3 to 30	10 to 100
Cycles/Burst	16	32

The seed material used was titanium dioxide having a nominal size of one micron. The ambient surroundings were not seeded. Standard fluidized-bed seeding techniques were used with the seed being introduced far upstream of the test section. The processor count rates varied from high levels on the order of 10,000 per second in the dense seed region to less than 10 per second at the periphery of the flow and in the vortex core at the nozzle discharge plane.

The nominal number of processed signals used to generate the velocity histograms was 512 per channel. Occasionally, levels up to 4000 per channel were employed when trouble shooting. At the periphery of the flow, where the velocities were less than 1 m/s, the flow was steady and laminar, and the data rates were very low, histograms based on as few as 200 counts were accepted.

A uniform time interval sampling mode was used to acquire the velocimeter data, except in the low seed concentration regions of the flow. A maximum data rate of 175 counts/sec was impressed by the system software such that the 512 measurements per channel were acquired in approximately three seconds. The velocity measurement should thus be regarded as time-averaged. The use of time-averaging as a means of suppressing velocity biasing in turbulent flows has been discussed by Craig et al (Ref. 30). No velocity bias corrections were applied during processing. All signals accepted by the velocimeter processor were used in the velocity determinations--no data editing was performed.

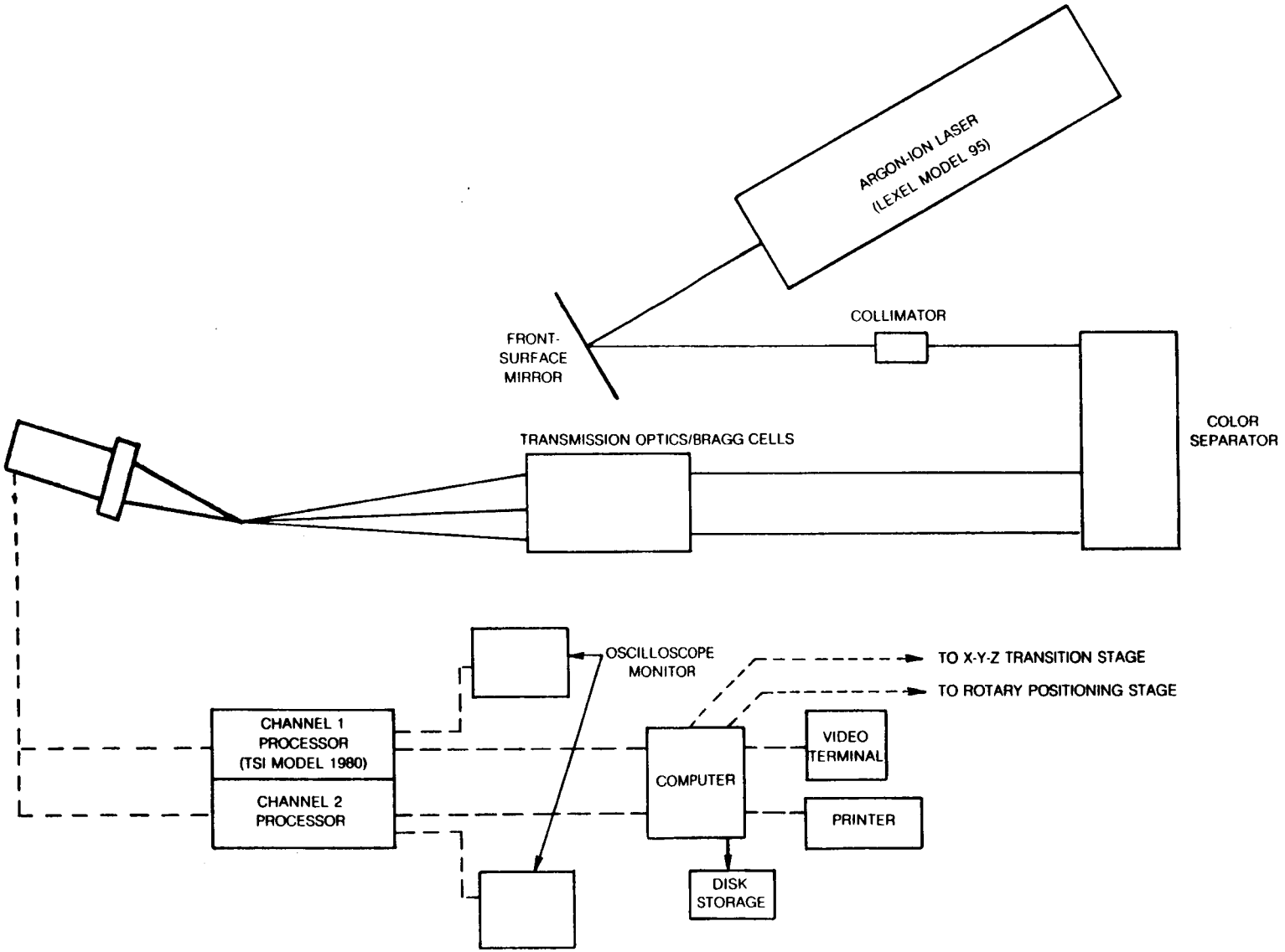

Figure 8. Laser velocimeter system.

Automated, precision positioning of both the test article and the velocimeter probe volume was used. A Partner III milling-machine equipped with a numerical control (CNC) system was employed to provide X-Y-Z translation of the velocimeter probe volume. This platform, on which all of the velocimeter components and the laser were mounted, provided the necessary precision, traverse range, stability and speed. Control of the machine was accomplished by the host system computer. This permitted integration of the software required for positioning with that required for activating the LDV processor. Rotation of the test article was accomplished by use of an instrument rotation stage (Daedel Model 20602) which was under the control of the host computer. Rotation of the nozzle permits flow asymmetries due to swirler non-idealities to be documented.

In order to locate the probe volume close to the nozzle to provide exit plane data, a small beam convergence angle in the horizontal beam pair was employed. This resulted in elongation of the probe volume. To reduce the length of the probe volume, off-axis collection optics were used. A forward-scatter, 30-deg, off-axis system with the collection optics rigidly mounted to the velocimeter platform was employed as shown in Fig. 5.

In order to permit the interpretation of the vertical component of velocity as the tangential or the radial velocity component, it is necessary to establish a reference axis for the flow. In a perfectly axisymmetric flow, the reference axis is the axis of symmetry. In a nearly axisymmetric flow, the axis can be either the geometric axis of the test article or an "aerodynamic center". (The aerodynamic center can be described by the location where the vertical component of velocity vanishes, or the location about which the velocity varies in a symmetric manner.) For these tests, the geometric center, based on measurements using fixtures inserted into the core flow passage of the nozzle, was used. Vertical positioning was established by observing the cut-off of the horizontal beam pair by a small diameter (0.8 mm) pin fixtured on the injector centerline (Fig. 9). The center was located by observing the extinguishing of the projected horizontal beam pair as the pin was approached from both an upward and a downward direction. Horizontal positioning was established by use of a fixture which positioned a thin, flat, transparent membrane at the fuel injector centerline. The scattering of the light forming the probe volume by the membrane was observed through a microscope objective placed in the LDV receiving optical train. Centering was obtained when the probe volume waist was imaged on the membrane. Axial positioning was established by observing the cut off of the vertical beam pair by the face of the fuel injector. The nozzle exit plane was fixed as the location at which the intensity of the projected vertical beams diminished to half the unblocked intensity.

The host system computer was a dedicated Apple IIe microcomputer. Custom machine language and BASIC software were used to drive the velocimeter processors, the three-axis velocimeter bed, and the rotary stage. Operation of the system was completely automated. During the experiment, the digital data from the two processors was reduced and histograms displayed in graphical form such that the test operator could note any abnormalities in histogram shape. Only the reduced data was stored on magnetic disk. Approximately 15 seconds were required to acquire, process, and store data required for 512-point

87 – 223A

ORIGINAL PAGE IS
OE POOR QUALITY

Figure 9. Beam alignment fixtures.

87 – 10 – 66 – 7

histograms on each of the two channels, and to position the equipment at the next measurement station.

Phase/Doppler Particle Analyzer

A phase/Doppler particle analyzer (Fig. 10) produced by Aerometrics, Inc. was used to obtain spatially-resolved information on particle size and velocity (Refs. 31, 32). The instrument is similar to a laser velocimeter in that crossing laser beams are used to define a probe volume in which interference fringes cause Doppler signals to be generated by moving droplets. Three detectors, rather than one, are employed using phase differences among the signals produced by the incident light to determine the droplet size. This phase difference depends on the index of refraction of the liquid phase, the viewing angle and the characteristics of the incident beams. It is assumed that the particles are spherical. The instrument was configured to capture forward scattered light, 30 deg off-axis (Fig. 5).

The instrument employed a single-channel; the transmitting optics were oriented in all tests such that the axial component of velocity was detected. Frequency shifting by means of a rotating diffraction grating was available such that negative velocities could be resolved. The 488mm beam produced by an Argon-ion laser operating at a power output of one watt was used.

Alignment of the phase/Doppler particle analyzer optical components was achieved by inspection of the envelope of the Doppler burst as displayed on an oscilloscope. For these alignment tests, which were performed on a daily basis, a piezo-electric aerosol generator was used to produce water droplets in the 1-5 micron size range, in the low velocity (less than 1 mps) flow generated by the action of the test chamber exhaust ejector. Alignment of the probe volume relative to the injector centerline and injector face was carried out in the same manner as for the velocimeter tests--by use of fixtures to block the incident laser beams.

Operation of the Aerometrics instrument requires that selection be made of appropriate values of velocity offset (grating rotational speed), velocity span (highand low-pass filter settings), size range (incident beam spacing and beam collimator focal length), and signal gain (PMT voltage). For these tests, a 300mm focal length collimator was generally employed. For the tests in which the liquid phase characteristics were measured, the signal gain was set to prevent PMT saturation by signals generated by the largest particles at each given traverse point. For the tests in which the gas phase characteristics were determined, signal gain was fixed at a relatively high level (PMT voltage of 300) to maximize the number of signals received from the smallest droplets. The other processor parameters were adjusted in order to maximize the number of valid data signals--valid data signals occur when the processed information yields a droplet size and velocity which lie within the limits specified by instrument settings. Upon completion of the acquisition of data at a particular point, the velocity and droplet size histograms were displayed to determine if the size or velocity distributions were cut-off by an inappropriate choice of instrument settings or by an inadequate instrument range. In the case where inadequate range causes cut-off, data-splicing techniques are available to combine data for multiple runs conducted with

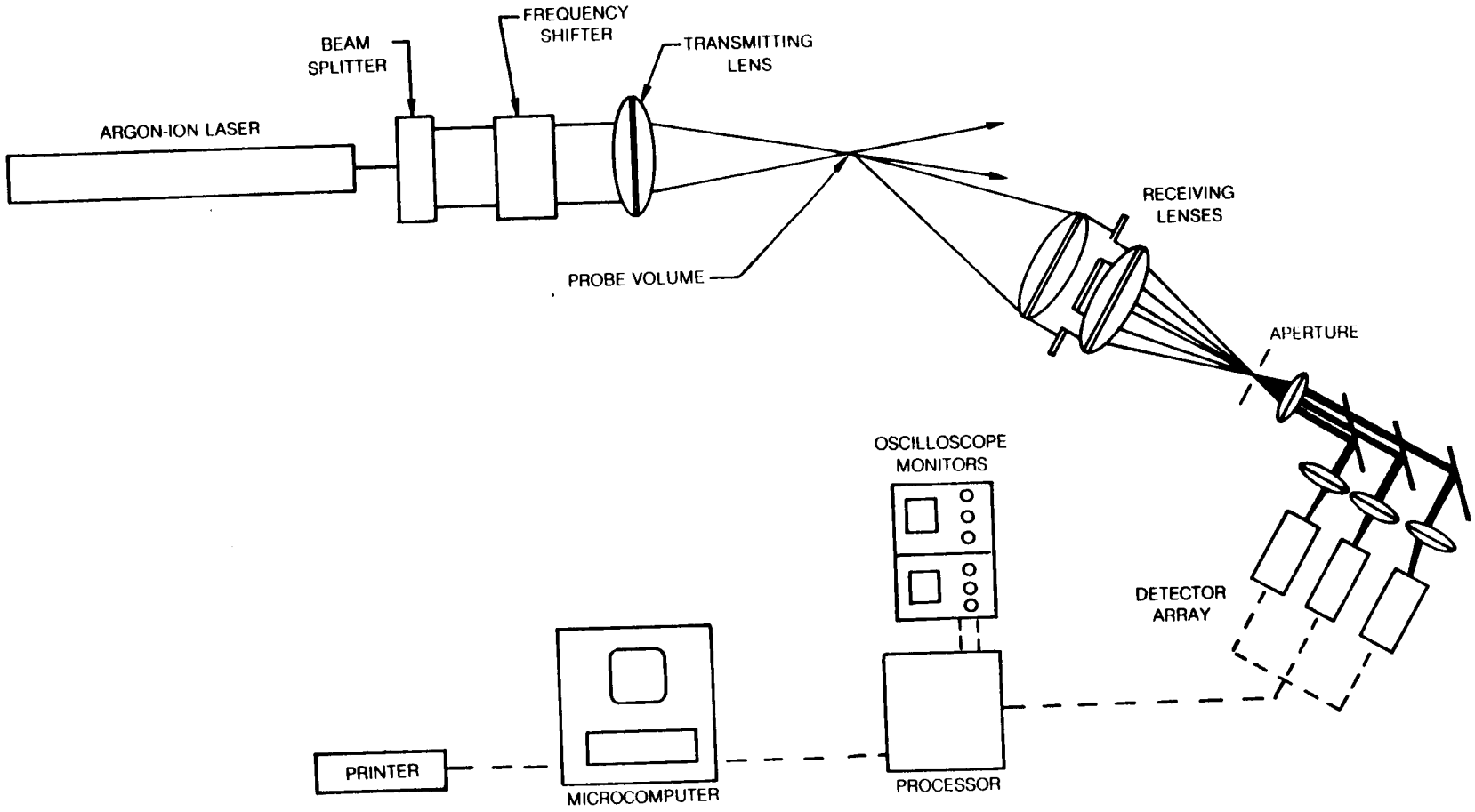

Figure 10. Phase/doppler particle analyzer.

87-10-66-8

different processor settings (Ref. 33). Such data splicing techniques were not employed, however, in this program.

The data rates achieved were high due to the high density of the spray--usually above 10000 counts/sec. The instrument was operated in a mode (the "DMA" mode) in which the data were transferred to memory, then processed. Processing ceased when the specified number of valid data points were validated--generally 5000 valid points were acquired.

The instrument provides correlated velocity/size data and therefore can provide a measure of the gas velocity as well as the spray velocity. In order to measure velocities of both phases, two horizontal traverses were conducted at each measurement station. The first traverse, with processor settings optimized to capture the entire range of velocities and particle sizes present, provided information on the spray droplet characteristics. The second traverse, with the instrument configured to obtain detailed information on the smallest particles, provided information on the gas-phase velocity in the presence of the spray. In this case, the velocity size histograms of the small particles were examined to insure that the velocity of the smallest particles varied in regular manner. That being the case, the data were extrapolated to zero size to yield a value of the gas-phase velocity. Generally, the velocity of the smallest particle (less than 5 microns) varied only weakly with size and this extrapolation could be performed by inspection. At the outer radii of the spray, the number of small particles produced by the spray was insufficient from a data rate viewpoint; therefore the outer flow was seeded in those tests. Various seed materials were investigated, droplets produced by a piezo-electric nebulizer proved most effective. For these phase/Doppler measurements, the technique employed was to seed only the external flow--not the flow passing through the swirler.

TEST CONDITIONS

The objective of this program was to gain information on the behavior of sprays under engine conditions. Tests, however, were to be conducted at ambient pressure conditions to avoid the expense of high-pressure testing. It is not possible to simultaneously preserve all of the significant parameters corresponding to engine operation when scaling from high pressure to ambient pressure. The procedure employed was to select the air-side pressure drop so as to produce the same air velocity as is generated by the swirler at the selected engine operating condition. The injectant flow is then established to preserve the liquid-to-gas momentum ratio. The parameter that is not preserved is the injectant flow rate. As a result, the velocity of the injectant at the discharge plane is lower during testing than during engine operation. Also, the loading ratio is lower. TEACH calculations showed the effect of the initial particle velocity on the spray distribution at these conditions was was small. The effect of the loading ratio on any possible interaction processes has not yet been determined.

The conditions selected for this program correspond to engine cruise operation (Table 2).

Table 2 Test Conditions

Injectant Flow Rate	71.4 kg/hr
Swirler Pressure Drop	70 mm Hg
Loading Ratio	0.7
Droplet Size Range	10-120 microns
Characteristic Velocity	125 m/s

RESULTS AND DISCUSSION

The axial stations at which data were obtained by use of the three different instruments are given in Table 3.

Table 3 Test Matrix

Station (cm)	Patternation		Velocimetry	Phase Doppler
	Water	Jet A		
.114			X	
1.27			X	
2.54	X	X	X	X
3.81	X	X	X	X
5.08	X	X	X	X
6.35	X	X		
7.62			X	
10.16			X	X

Spray Patternation Data

The results of the spray patternation tests using water as the injectant are given by the contour plots of Fig. 11. Measures of circumferential uniformity are provided by the patternation index, PI. The mass flow in each of eight 45-deg sectors can be used to calculate the value of the "Patternation Index" (Ref. 26); the values of 5.5 to 7.4 obtained for this nozzle are indicative of a highly circumferentially uniform spray. Of course, a perfect nozzle would exhibit circular contours. Values of this and other measured parameters at the four stations are given in Table 4.

Table 4 Patternator Results

Measurement Station (cm)	Water				Jet-A			
	2.54	3.81	5.08	6.35	2.54	3.81	5.08	6.35
Patternation Index	5.8	6.2	7.4	6.7	9.3	9.1	8.4	8.1
Spray Angle (deg)	85	75	69	64	70	61	57	54
Collection Efficiency	1.09	1.06	1.03	0.96	0.88	0.88	0.88	0.88
SMD (microns)	76	70	63	57	27	25	23	22

A spray angle equal to the included angle of a cone which intercepts both the nozzle filmer lip and the circle encompassing 90% of the spray mass flux at the measurement station can be calculated. The measured angle of 85 to 64 deg varied varied with axial distance in a manner characteristic of a bell-shaped envelope.

The values of SMD recorded by the Malvern ST1800 are shown to vary from 76 to 57 microns. No attempt has been made to analyze the cause or significance of this variation. It is pointed out that these measurements are line-of-sight measurements performed in regions of varying spray density where

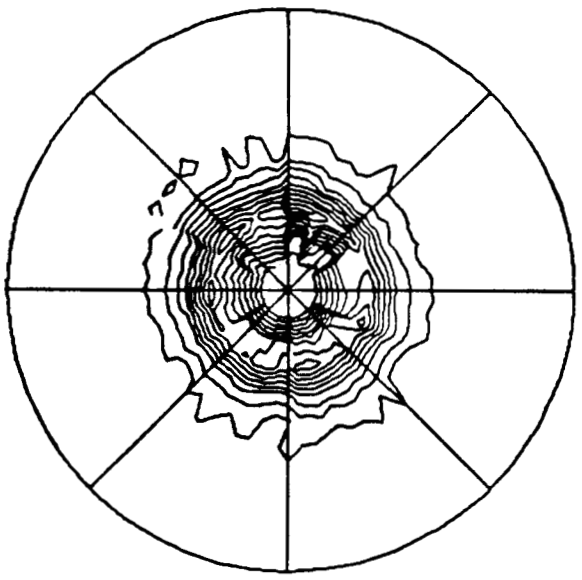

Z = 2.54

PI = 5.5
Min/Max = 0.75
CE = 1.06
Alpha = 85
SMD = 76

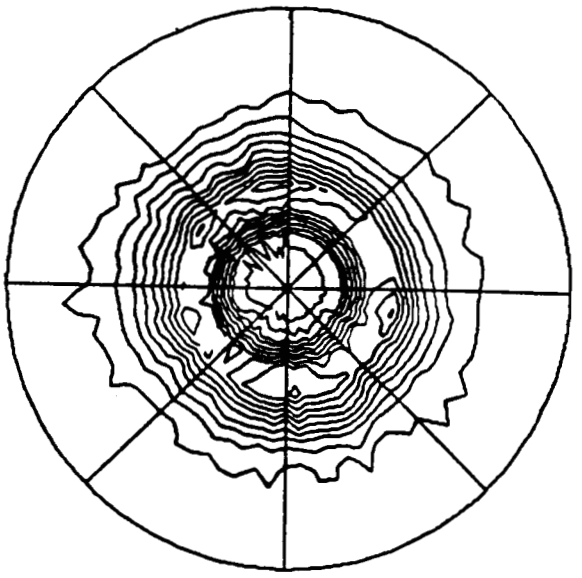

Z = 3.81

PI = 6.2
Min/Max = 0.79
CE = 1.06
Alpha = 75
SMD = 70

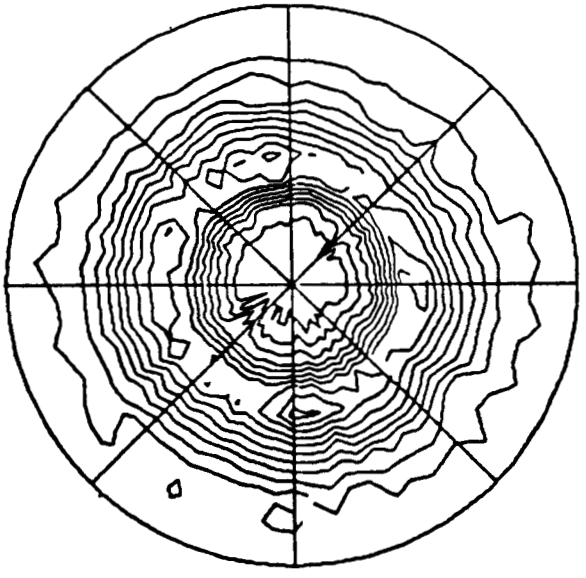

Z = 5.08

PI = 7.4
Min/Max = 0.76
CE = 1.03
Alpha = 69
SMD = 63

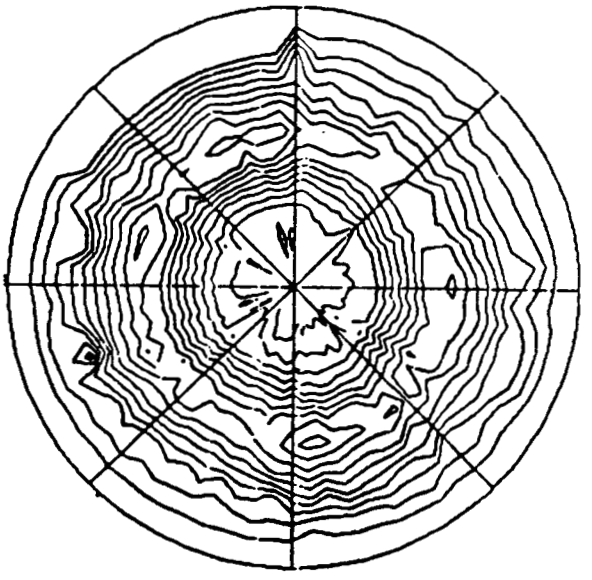

Z = 6.35

PI = 6.7
Min/Max = 0.76
CE = 0.96
Alpha = 64
SMD = 57

Figure 11. Mass flux distribution — Water.

87-10-66-16

there are large velocity differences between large and small particles. The implications of these flow characteristics on line-of-sight measurements have been discussed by Dodge (Ref. 34).

The collection efficiency of the patternation system varied from 1.06 to 0.96. This value is the ratio of the integrated flow rate to the metered flow rate; the values shown are larger than the range of 0.8 to 0.85 generally obtained in this apparatus for Jet-A (not water) sprays (Ref. 26). The greater efficiency was probably associated with lower carry-over losses due to non-isokinetic sample collecting when sampling sprays having a larger mean droplet size.

The radial distribution of mass flux for the water spray obtained at the four measurement stations is given in Fig. 12. The plotted data points represent the mean of the 72 data points acquired at each of the ten sampling probe radii. The hollow cone nature of the spray is evident.

Patternation tests were also conducted with Jet-A fuel during the process of selecting the nozzle components which would provide the highest degree of circumferential uniformity. Results for the selected configuration using Jet-A are shown in Fig. 13. Comparison of these results with those obtained using water show that the circumferential uniformity indices are slightly poorer, the spray angle is somewhat smaller, and that the SMD is greatly reduced. The 20-30 micron level for SMD obtained with Jet-A is of the level routinely measured for this type of nozzle. The radial mass flux distribution shown in Fig. 14 is similar to that obtained using water.

Laser Velocimeter Data

The velocity profiles at the most upstream measurement station (Z=0.114 cm) are shown in Fig. 15. The existence of a central vortex cone region of low velocity is made evident by the axial velocity profiles. The steepness of the velocity gradient in this region is notable as is the fact that the centerline mean velocity is not strongly negative. The centrifugal force field established in the central vortex was of such strength that, when conducting the experiments, the micron-sized titanium dioxide seed particles were totally centrifuged from this region. In order to obtain information on the nature of the central region velocity profile, the swirler pressure differential was reduced until the data rates in this region were acceptable. The profiles in this region were found to have a very distinct shoulder that was always located at r=$\pm$0.1 cm; the velocity profiles measured at the reduced pressure drop (4.67mm Hg) were multiplied by the ratio of these shoulder velocities to scale the data to the Baseline pressure differential level.

The diameter of the high axial flow velocity region (above 60 m/s) is 1.7 cm, compared to the end cap diameter of 2.0 cm. This slight convergence of the flow area in the upstream region is consistent with visual observations of the envelope of the fuel spray produced by this type of injector.

The measured tangential velocity profile at the exit plane is shown in Fig. 16. The anti-symmetric pattern is the expected profile for a nearly axisymmetric flow. The notable features are the steep velocity gradient in the vortex core, the double-peaked structure in the high velocity region, and the apparent reversal of the swirl direction in the outer, low-velocity region

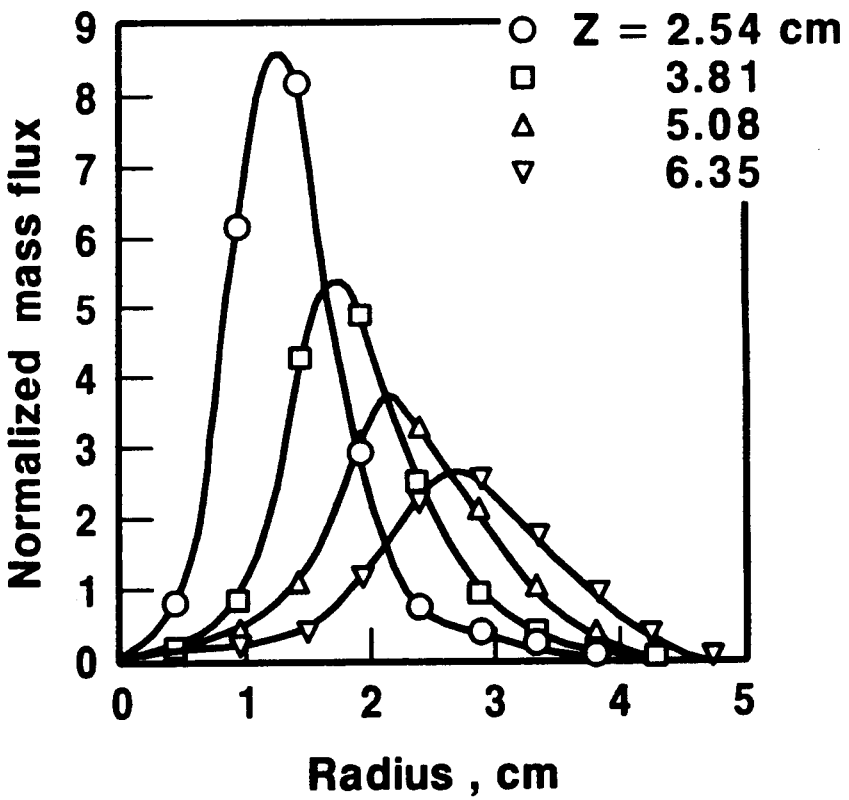

Figure 12. Radial mass flux distribution — water.

87-10-66-9

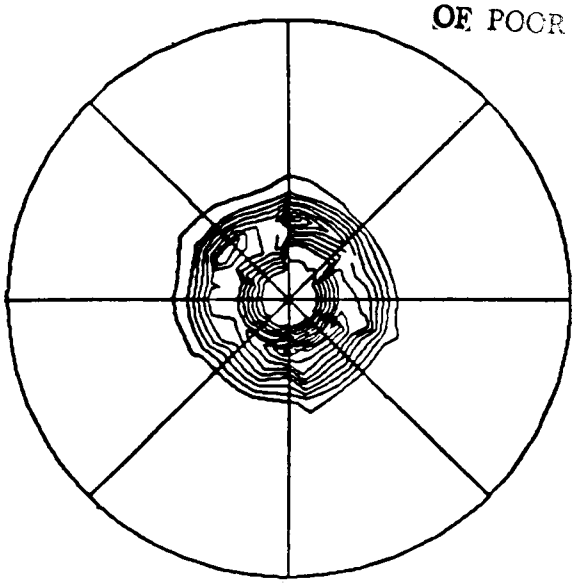

Z = 2.54

PI = 9.3
CE = 0.88
Alpha = 70
SMD = 27

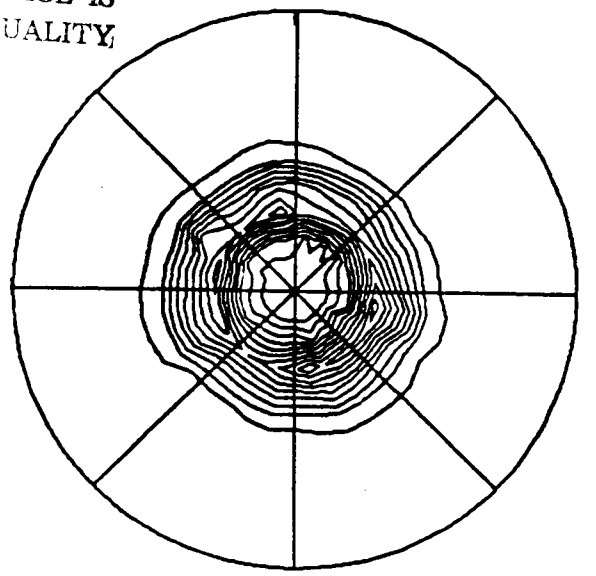

Z = 3.81

PI = 9.1
CE = 0.88
Alpha = 61
SMD = 25

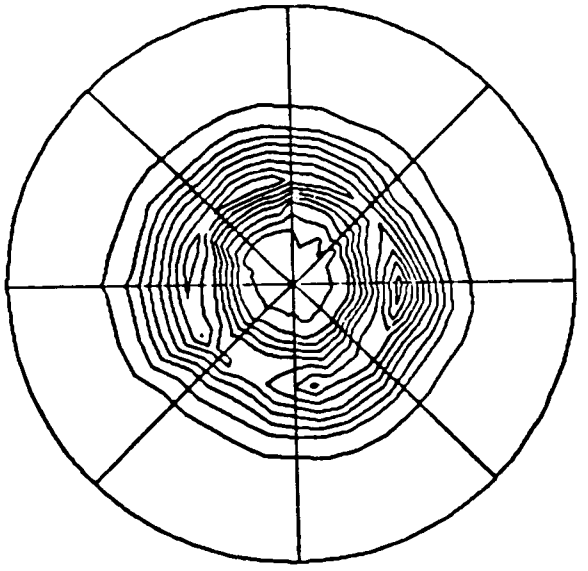

Z = 5.08

PI = 8.4
CE = 0.88
Alpha = 57
SMD = 23

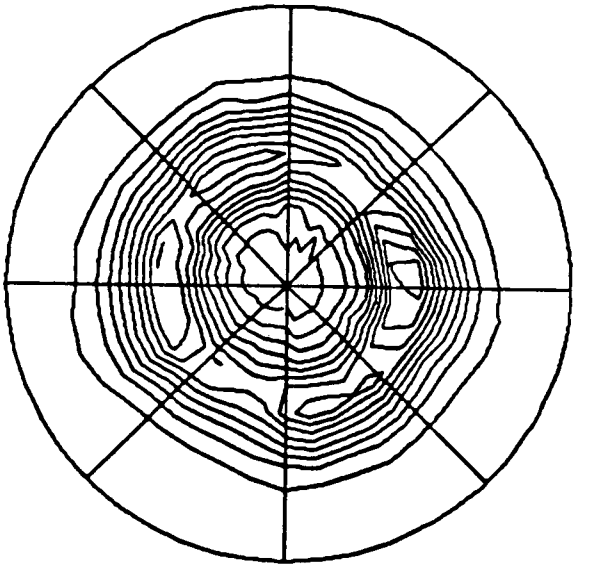

Z = 6.35

PI = 8.1
CE = 0.88
Alpha = 54
SMD = 22

Figure 13. Mass flux distributions — Jet-A.

87-10-66-17

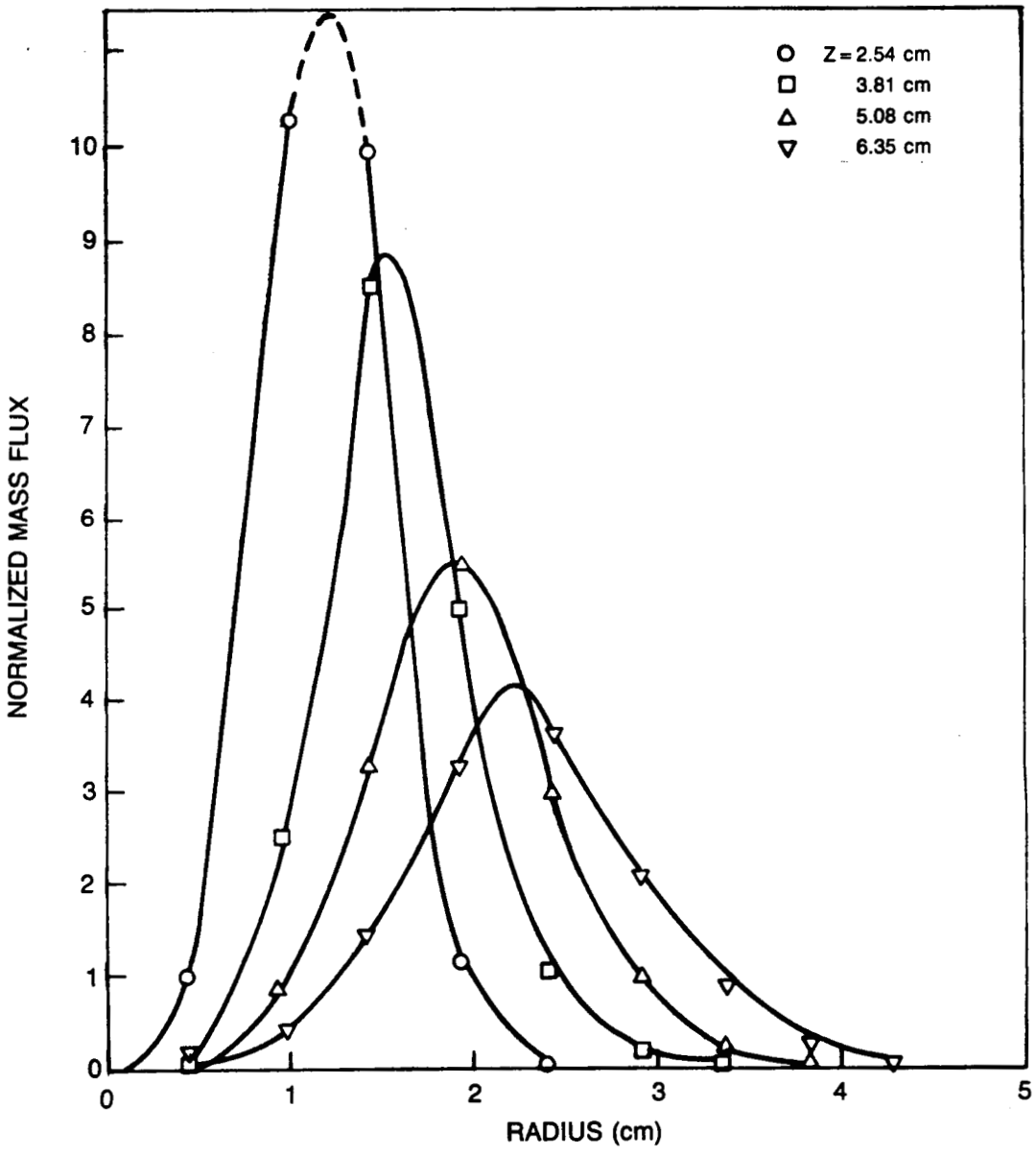

Figure 14. Radial mass flux distribution — Jet-A.

87-10-66-10

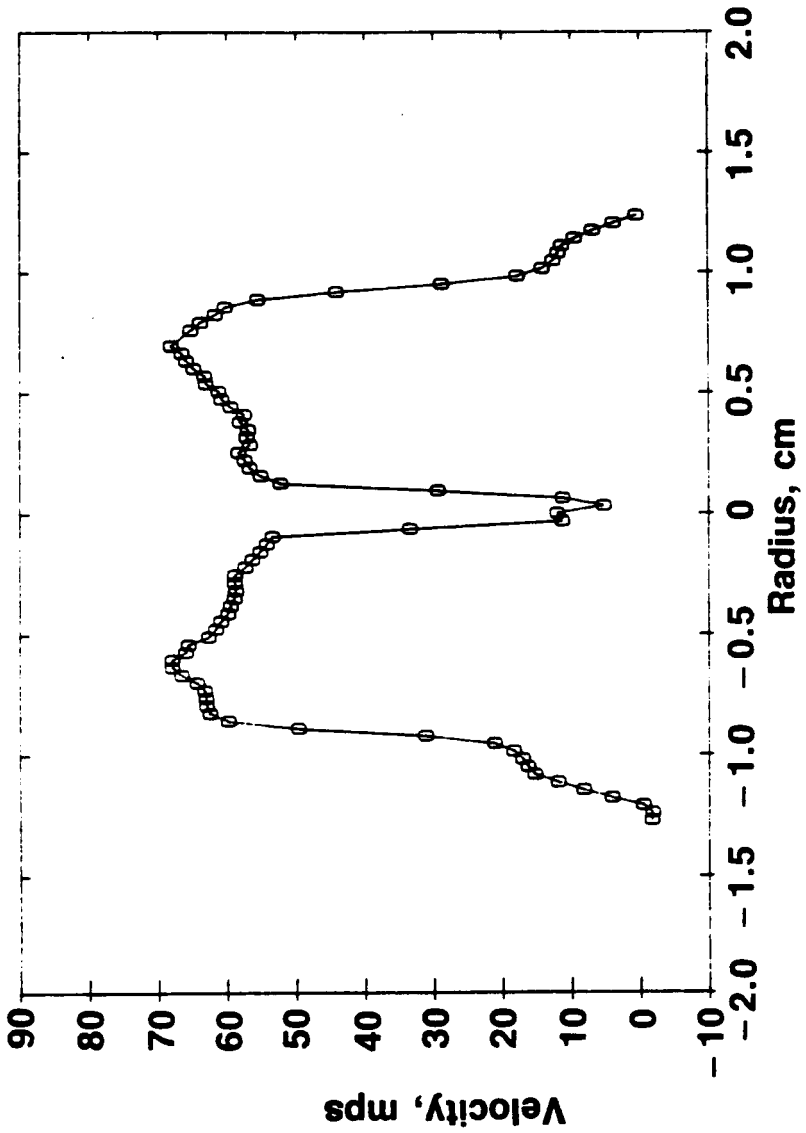

Figure 15. Exit plane axial velocity.

87-10-66-11

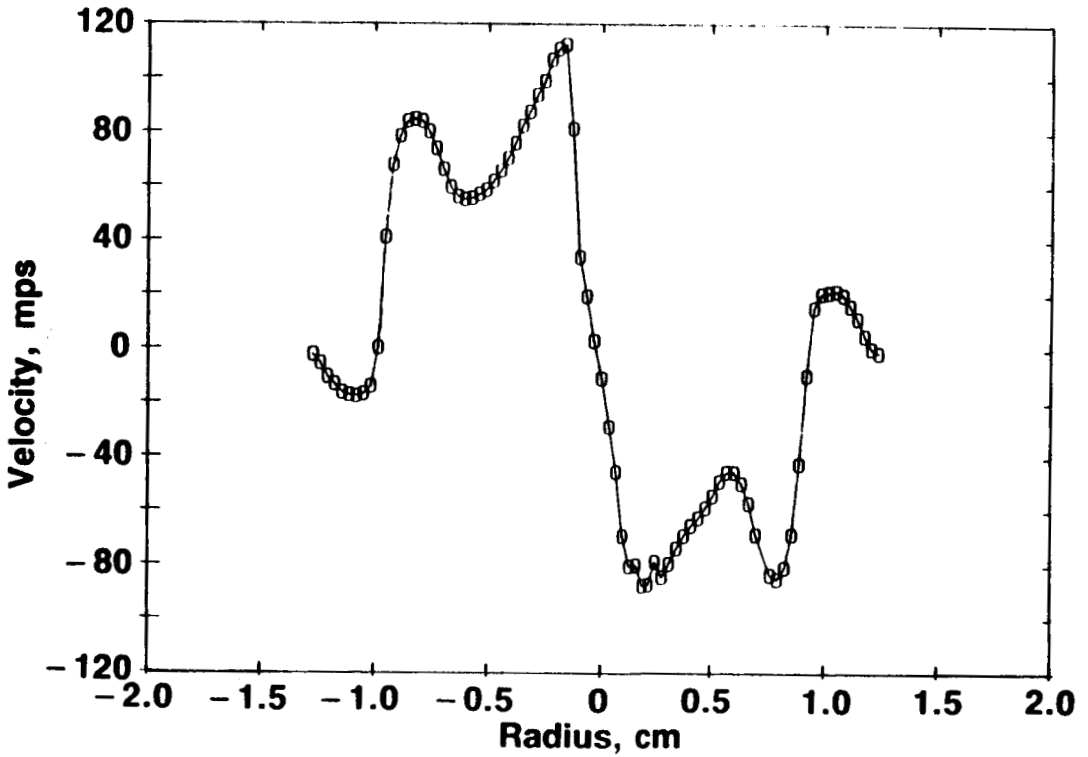

Figure 16. Exit plane tangential velocity.

of the flow. Also evident is a degree of asymmetry in the data pattern which is most noticeable in the magnitude of the peak velocities occurring at the edge of the vortex core. Such asymmetries in the measurement of the tangential component of velocity of a nominally axisymmetric flow can be evidence of biasing in the velocimetry data due to the higher fringe-crossing rate when the gas velocity opposes the direction of fringe motion (imposed by the frequency shift) than when the gas and fringes move in the same direction. To minimize this effect, the frequency shift was maximized (40 MHz compared to a Doppler frequency of 18 MHz) and the number fringe crossings for data validation was set to the highest possible value (32). The secondary velocity peaks do not exhibit this asymmetry (values of 84.6 and 85.1 m/s being measured).

The apparent reversal of the sense of rotation of flow in the outermost region of the flow displayed by the data is curious. The probability distribution function (pdf) for velocity in the region shows a distinctly bi-modal behavior (Fig. 17) with the average velocity of the major peak being zero. Because this behavior was noted in measurements at the plane closest to the nozzle discharge, signal biasing due to reflections was suspected. However, the magnitude of the Bragg cell velocity offset and the fact that the sign of the velocity associated with the minor peak is different at the near and far boundaries do not support this contention. Given the experimental configuration--a rotating free jet--no external mechanism for establishing a counter-rotation in the external flow is apparent.

The radial velocity measured at the exit plane was of a smaller magnitude than the axial and tangential components (Fig. 18). The radial velocity is directed radially inward (negative velocity at negative values of radius [negative value of y] translates to radial inflow; see Fig. 6) as a result of the action of the swirler end cap. It proved to be very difficult to measure accurate values of radial velocity in the region near the vortex core. This was probably associated with the unsteady behavior of the vortex core (Ref. 35), coupled with the fact that as the center of rotation shifts off the geometric center, the measured vertical component of velocity will contain a component of the large-magnitude tangential velocity. Furthermore, the existence of large velocity gradients, and high turbulence levels (which lead to substantial changes in flow direction relative to the fringe pattern within the finite probe volume) can be expected to lead to accuracy degradation (Ref. 36).

The ratio of the tangential to axial velocity defines the swirl angle (Fig. 19) which is shown to vary from approximately 45 to 75 deg in the main region of the flow. Indeed, it is expected that the swirl angle would be greater than the 40-deg outer swirler vane exit angle due to contraction imposed by the swirler end cap. The outer region data reflect the sign reversal noted earlier.

The swirl number, defined as the ratio of the tangential momentum to the product of the axial momentum and the radius of the outermost data point, was calculated to be 0.5. No accounting was made for the pressure-area term contribution to the axial momentum (the exit plane static pressure distribution was not measured). The mass flow calculated by integration of the axial velocity distribution was 0.025 kg/sec; this value is about 80% of the flow delivered to the plenum enclosing the injector in the patternation tests. This 80% figure is reasonable since no attempt was made to fully seal that

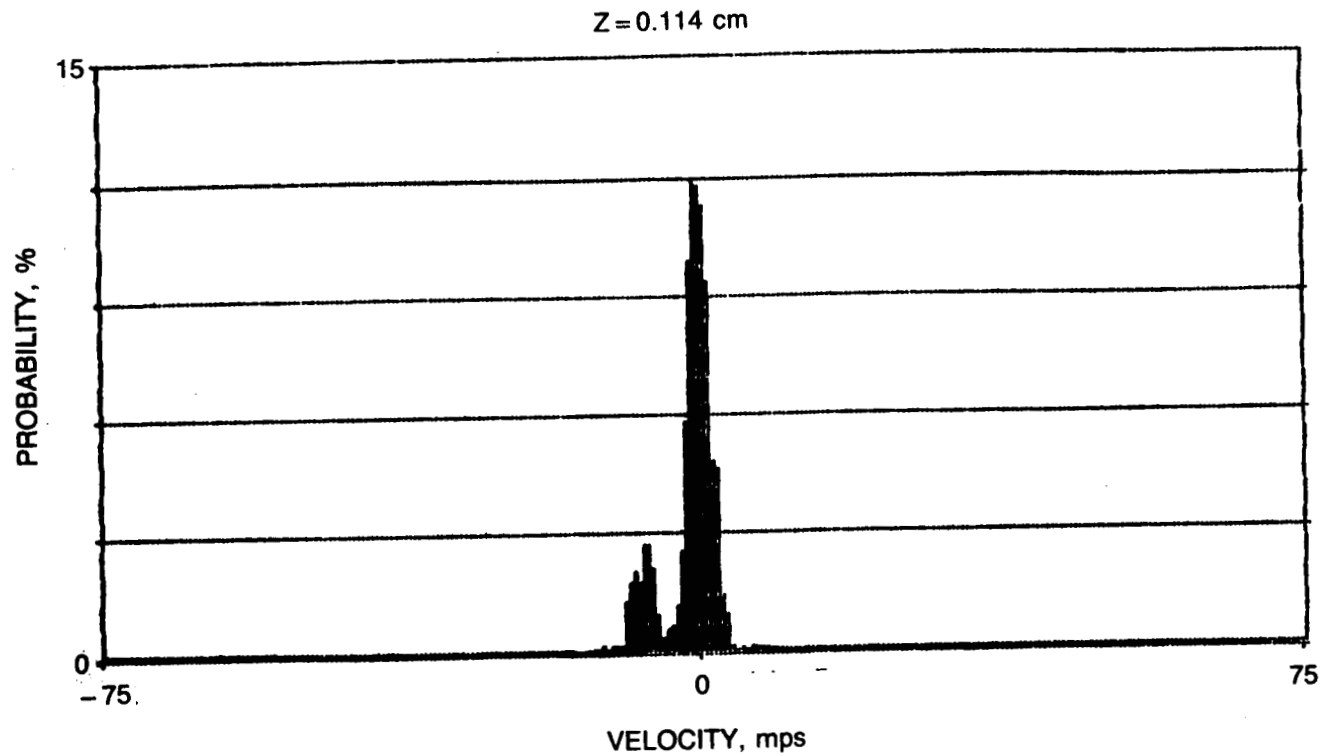

Figure 17. Bimodal tangential velocity probability distribution function at jet boundary.

87-10-66-28

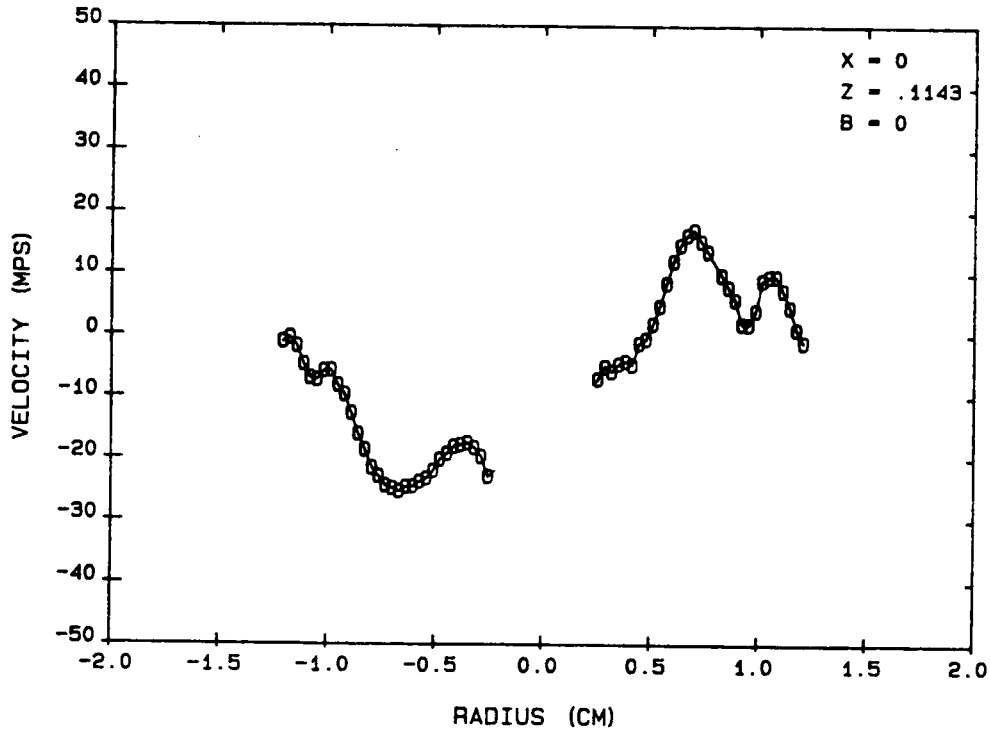

Figure 18. Exit plane radial velocity.

87-10-66-18

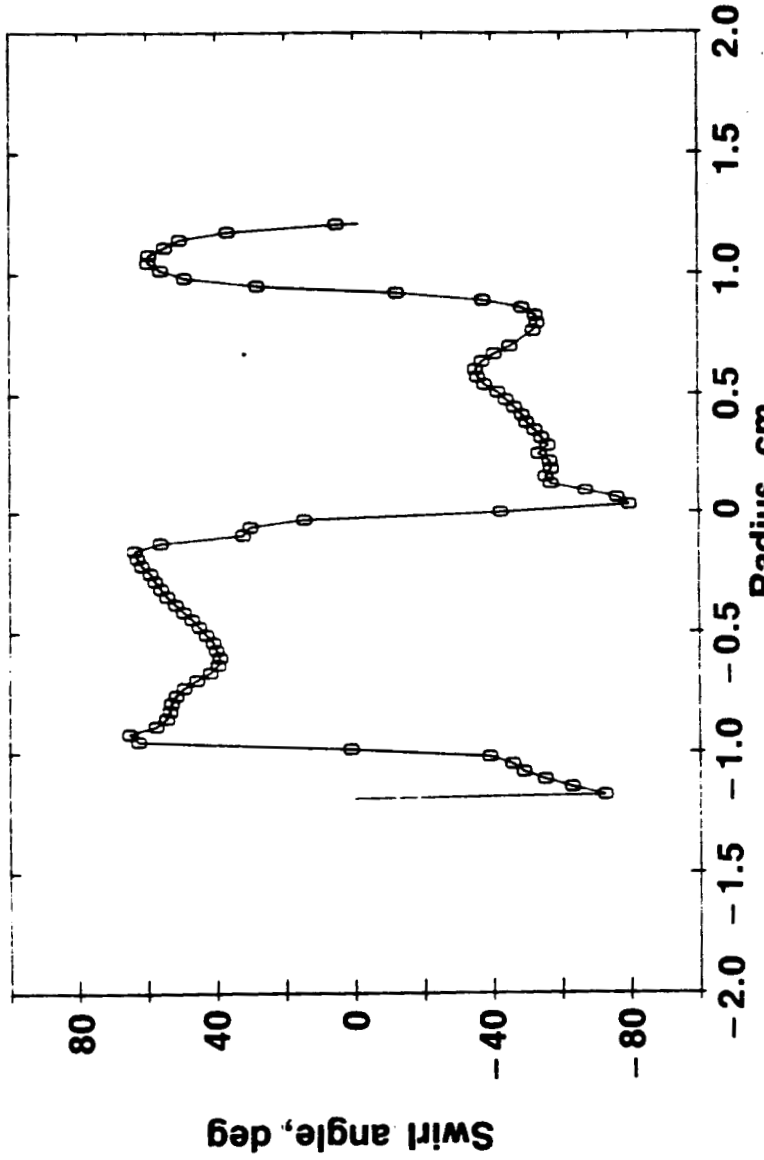

Figure 19. Exit plane swirl angle.

87-10-66-13

plenum (the test conditions are set by establishing the swirler pressure differential, not the mass flow).

The rms values of the fluctuating velocity components at the exit plane are shown in Fig. 20. As expected, high levels exist in the high shear regions, particularly the vortex core. In the main body of the flow, the fluctuating velocity varies between 10 and 20 m/s.

Because the injector assembly can be expected to produce wakes from the discrete number of swirler vanes, a series of tests were conducted in which the nozzle was rotated in increments of 30 deg. Results of the axial and tangential velocity measurements are shown in Fig. 21. No substantial wake effects were detected.

The results of axial velocity measurements at successive downstream measurement locations are shown in Fig. 22. At all downstream locations, there was sufficient seed in the central vortex to permit acquisition of data at the full swirler pressure drop of 70mm Hg. The expected trends are evident with the profiles exhibiting satisfactory symmetry.

The results of the measurements of the tangential velocity distribution in the downstream regions are shown in Fig. 23. The most significant abnormality is the asymmetry which suggests that the aerodynamic center lies at a value of r=-0.2 to -0.3 cm relative to the geometric center. This anomaly was recognized early in the test effort and led to several reviews of the equipment alignment procedures. The runout of geometric axis of the test article relative to the traverse axis was determined to be 0.05mm over a run of 10 cm and thus misalignment cannot be identified as an error source.

The downstream radial velocity profiles, Fig. 24, show that there is a radial outflow in the downstream region as opposed to the inflow observed at the discharge plane. This observation is consistent with the decay and flattening of the axial velocity profile and the resultant growth in the jet diameter.

Measurements were also obtained of the mean velocity components at the lateral boundary of the jet. The objective was to obtain information which could be used to establish a boundary condition when modeling this unconfined flow. The geometry of the lateral boundary was that of a conical surface intersecting the coordinates r=0.45, Z=0 and r=2.0, Z=10.16 cm. It is recommended that along this boundary the following values of velocity component be assigned:

$$\begin{aligned} \text{Axial velocity} &= 2 \text{ mps} \\ \text{Tangential velocity} &= 1 \text{ mps} \\ \text{Radial velocity} &= 2 - 0.15 \times Z \text{ mps} \end{aligned}$$

where Z is the distance (cm) downstream of the nozzle face and the sense of the radial component is everywhere inward.

Phase-Doppler Anemometer Data

PDA data were acquired at four downstream stations. Attempts to acquire data at a distance of less than 1.27 cm from the injector were unsuccessful

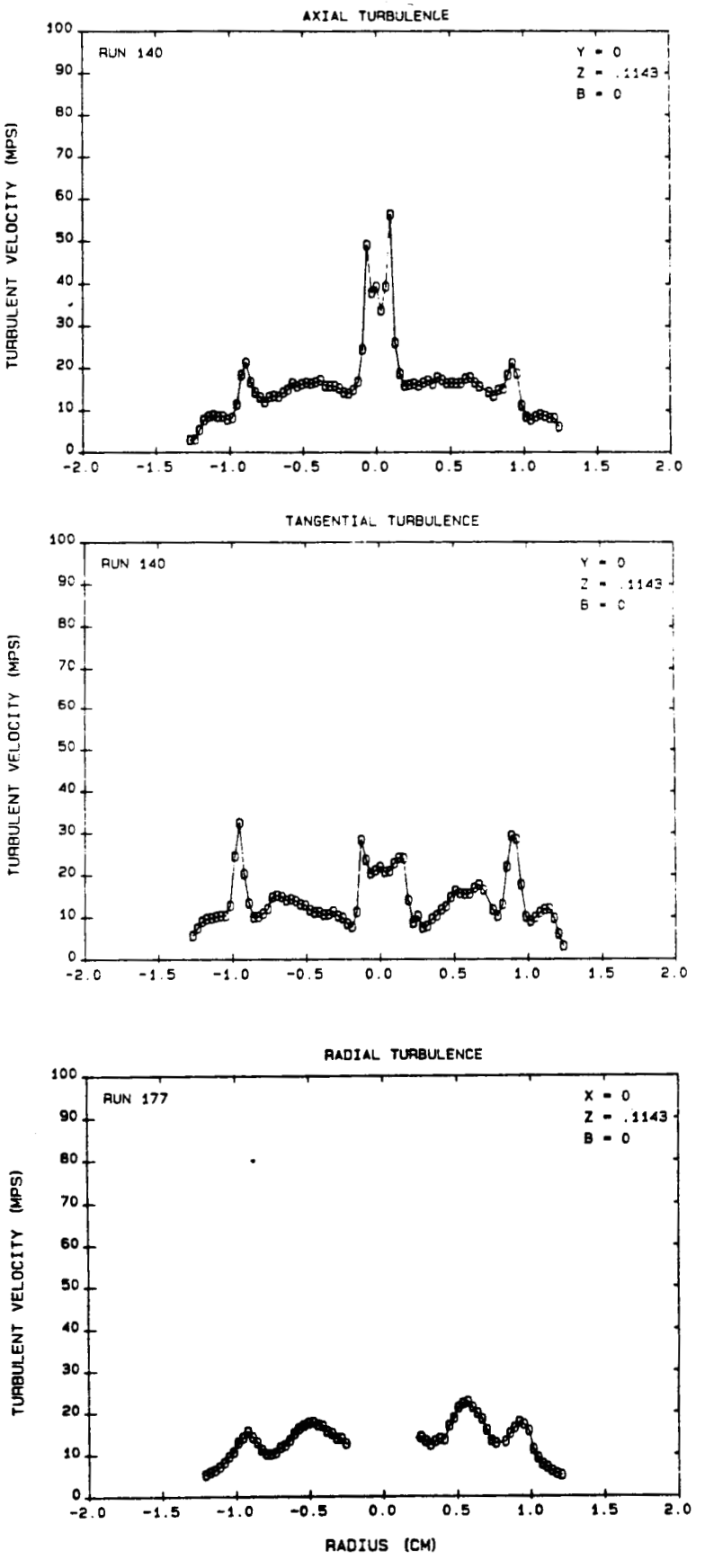

Figure 20. Exit plane RMS velocity profiles.

87-10-66-23

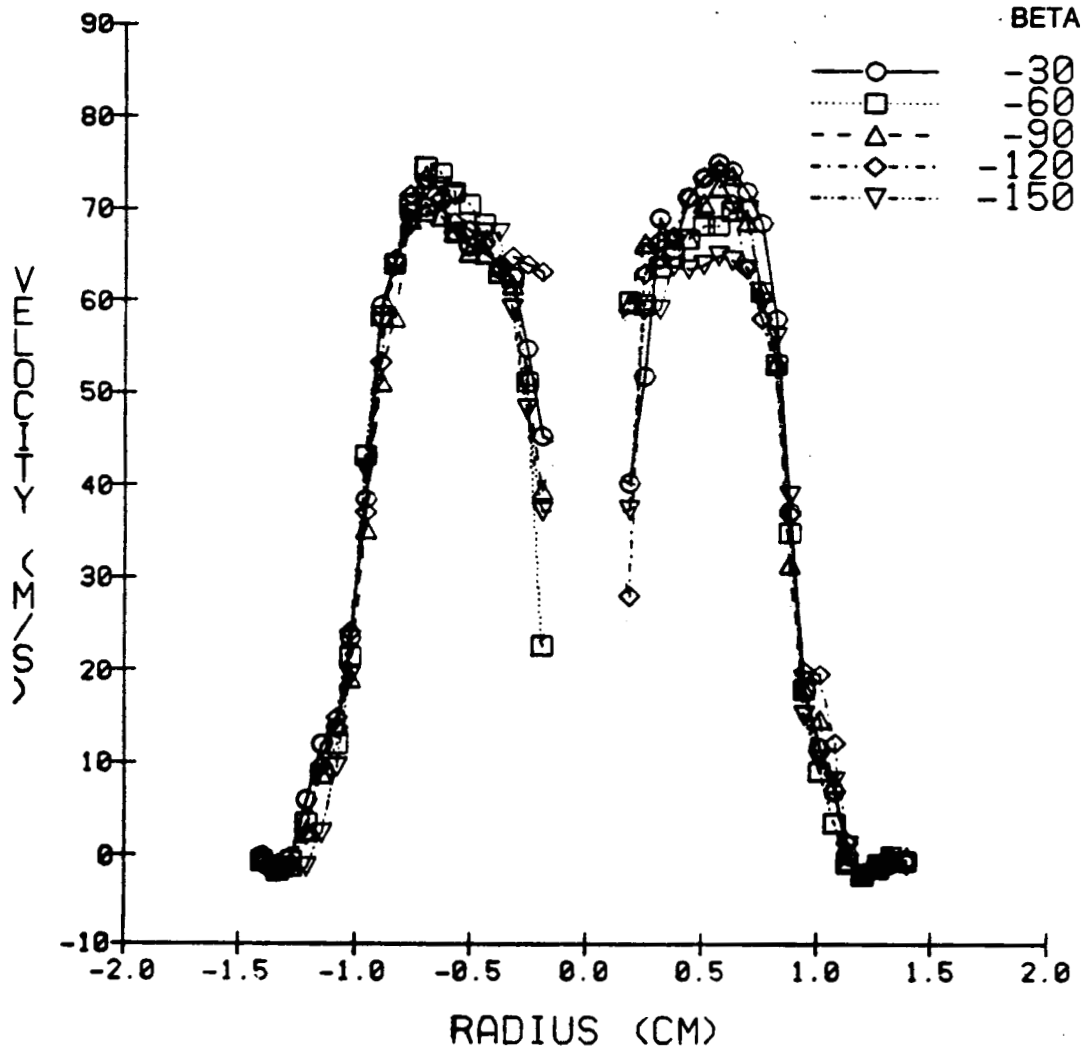

Figure 21. Effect of injector azimuthal position on exit plane axial velocity.

87-10-66-29

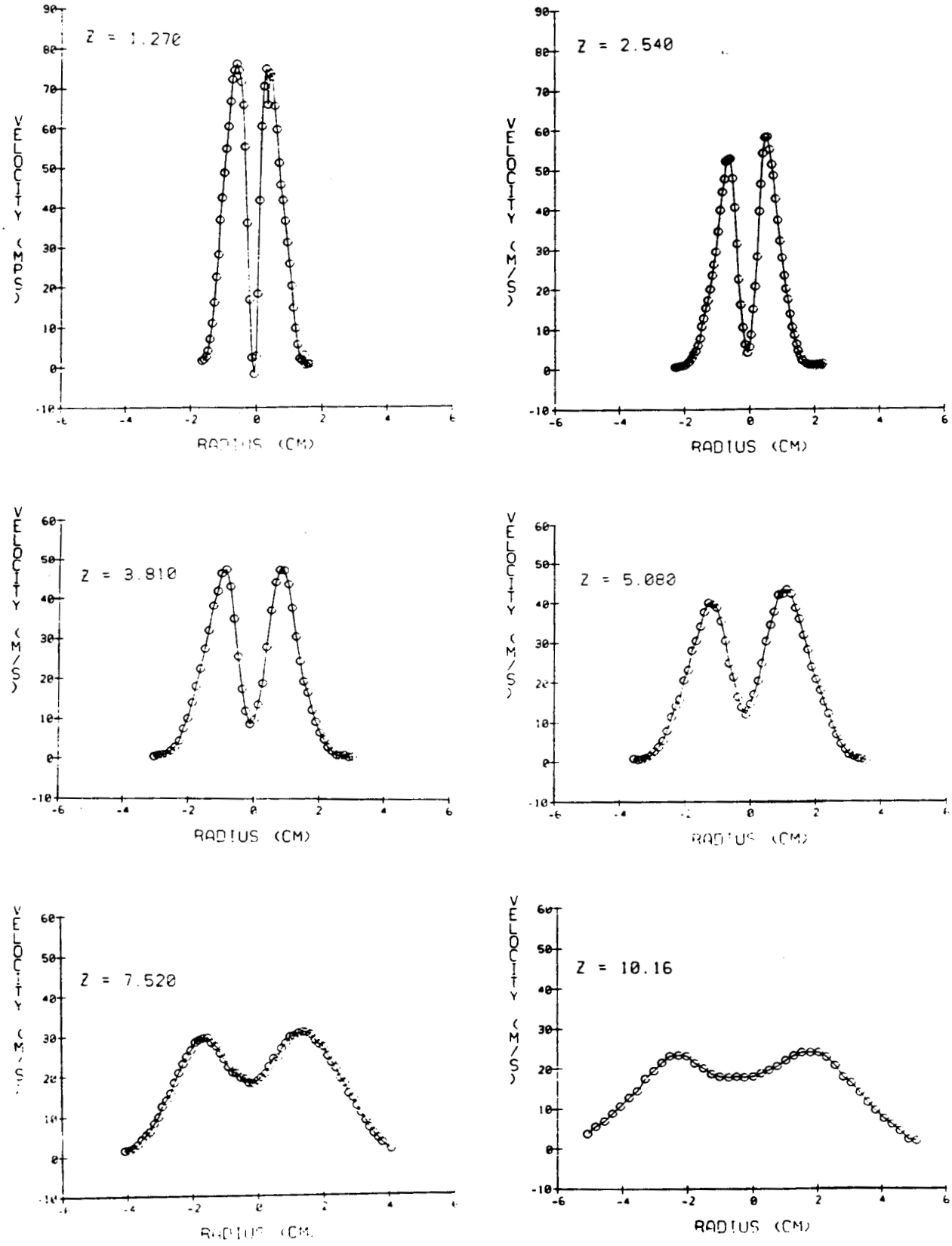

Figure 22. Downstream swirler flow profiles — axial velocity.

87-10-66-22

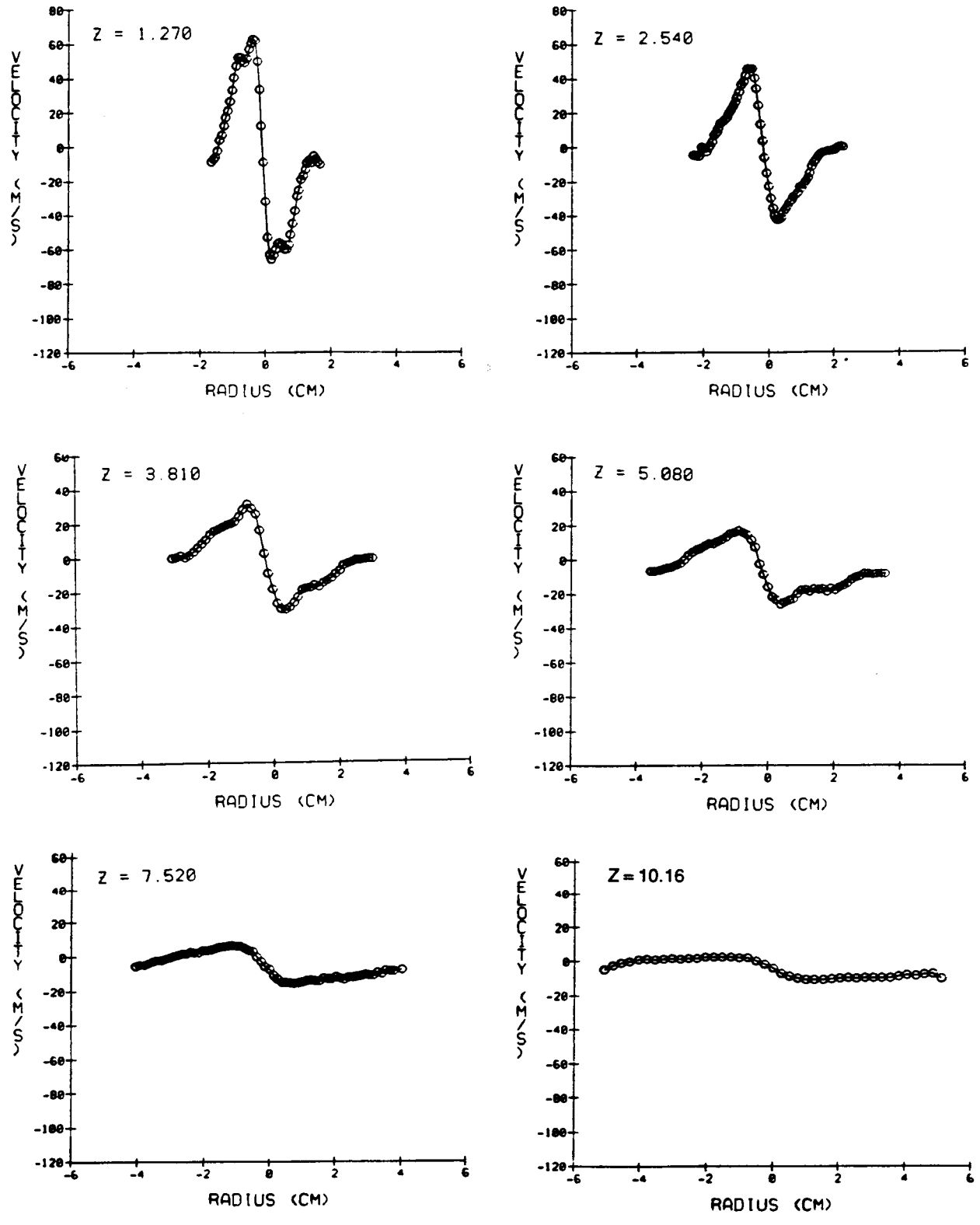

Figure 23. Downstream swirler flow profiles — Tangential velocity.

87-10-66-24

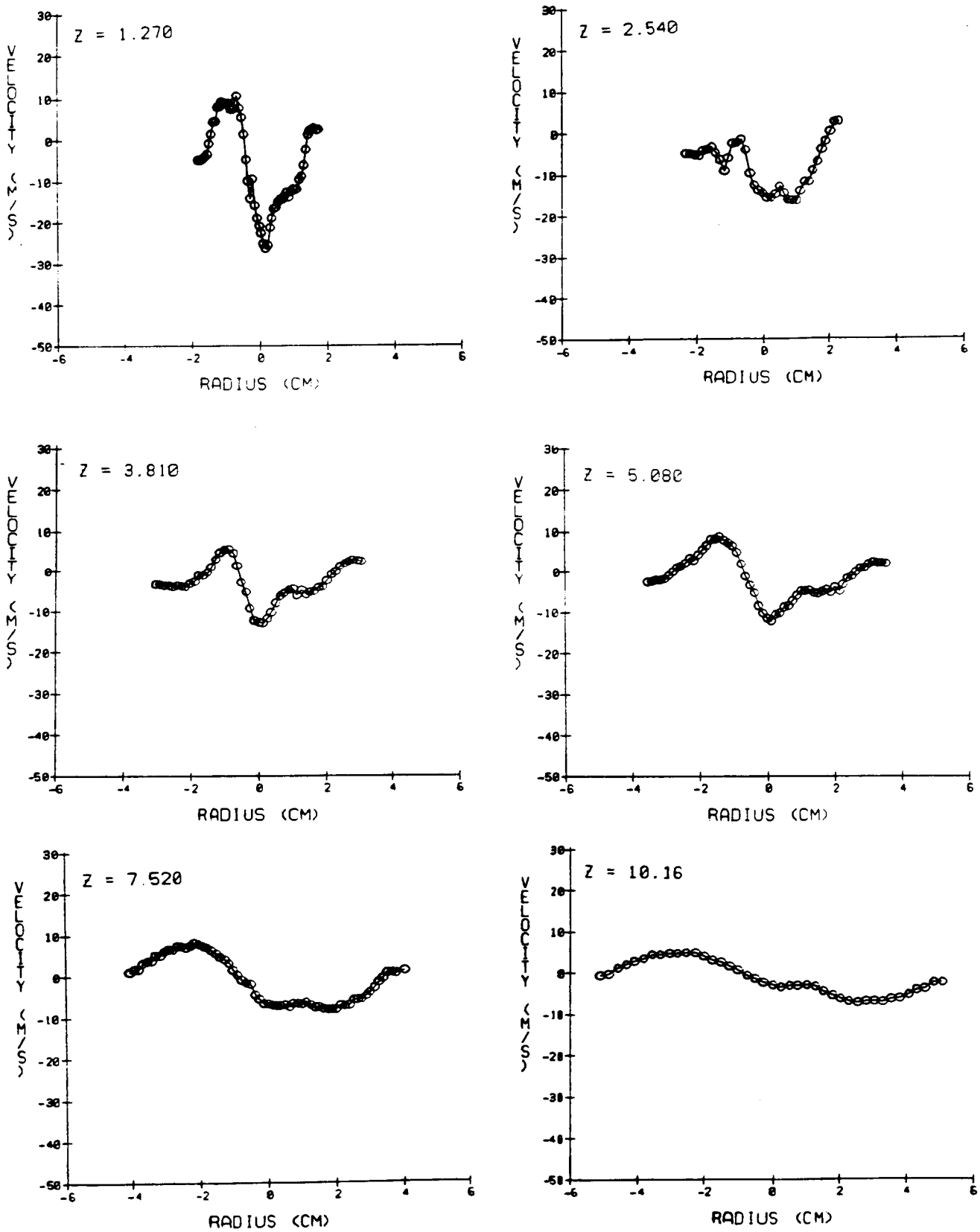

Figure 24. Downstream swirler flow profiles — radial velocity.

87-10-66-27

due to the very high data rejection rates. The highest indicated droplet number densities for which data were obtained were of the order of 10^4 droplets/cc.

Examples of PDF's showing the number distributions of velocity and droplet size and the size-velocity correlations produced are given in the Appendix.

Velocity

The distribution of mean axial velocities is shown in Fig. 25; data acquired using the LDV system for the gas velocity in the absence of the spray are also shown in the figures. Comparison of the gas-only (#-symbol) and the gas-phase velocities in the presence of the spray (X-symbol) at the three upstream stations show that, at each station, the profiles are virtually identical except in the center of the flow where the velocity depression associated with the vortex core has been moderated. This feature is consistent with a flow situation in which these central region droplets are accelerated to a high velocity immediately downstream of the nozzle, but thereafter decelerate less rapidly than the gas.

The liquid phase (O-symbol), which is the average of the velocities of all particles, is shown to have a non-zero velocity in the outer region of the spray where the gas phase is essentially quiescent. This is due to the larger droplets being centrifuged to the outer region of the spray. In the interior of the spray the liquid phase velocity is greater than the gas-phase velocity. Between this interior region and the external region, an annular region exists for the three most upstream locations in which the gas and liquid-phase axial velocities are nearly identical. This is not observed at the most downstream location. At the most downstream location, a significant difference between the spray-on and spray-off profiles is observed--the breadth of the gas-only jet is greater than in the case of the spray. Whether this is a manifestation of the effect of a reduced jet entrainment rate caused by a moderation of the turbulence levels or is a result that can be explained on the basis of droplet-gas momentum exchange due to velocity lag considerations remains to be determined.

A measure of the extent to which the level of the gas-phase velocity fluctuations can be effected by the presence of the spray is afforded by the PDA information obtained using the seeded spray. In this case the seed particles were produced by a piezo-electric nebulizer, and differ from the titanium dioxide particles used in the LV measurement in their ability to respond to turbulent fluctuations. The measured droplet sizes for the four smallest-diameter bins (out of 50) ranged from 1.4 to 4.4 microns. A representative value of the RMS velocity obtained from inspection of the statistical information for these four bins is compared with the RMS velocity obtained in the LDV for the gas-only case tests for the Z=5.08 cm station in Fig. 26. As expected, the turbulence level is lower in the case of the spray.

Droplet Size

The Sauter mean droplet diameter at each radial measurement station is shown in Fig. 27. As expected, a substantial range of droplet sizes is observed as the largest droplets are centrifuged to the periphery of the spray. In the interior of the flow, the SMD is on the order of 10-20 microns.

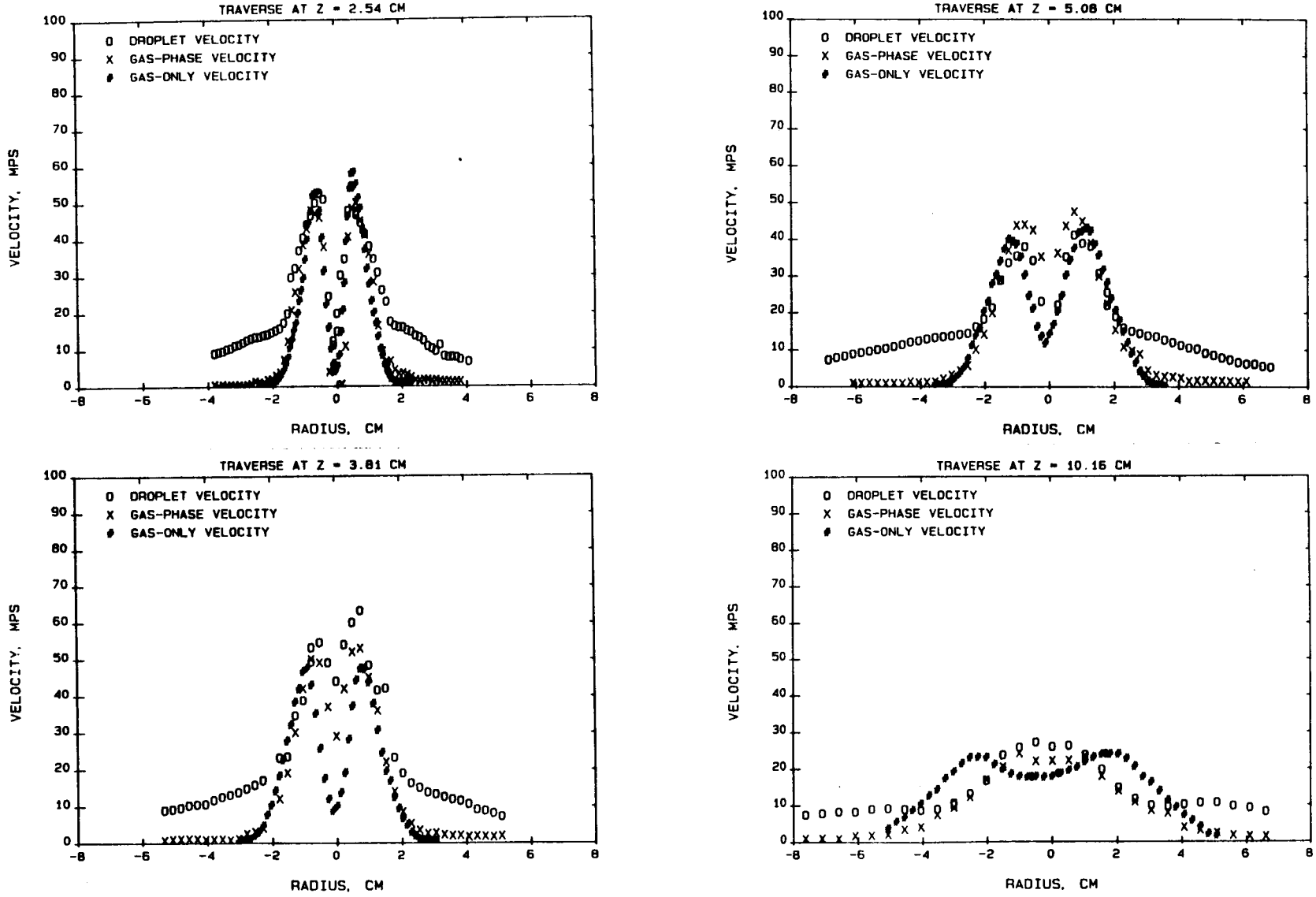

Figure 25. Spray axial velocity field

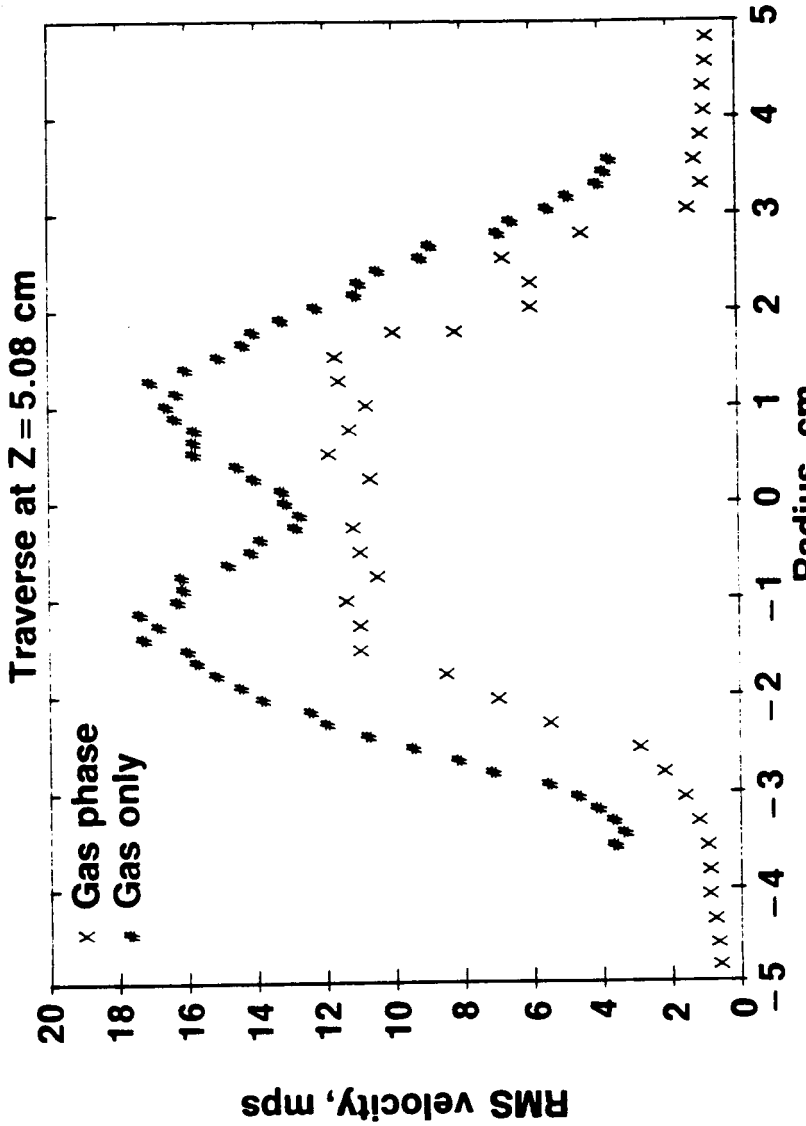

Figure 26. Axial turbulence.

87-10-66-15

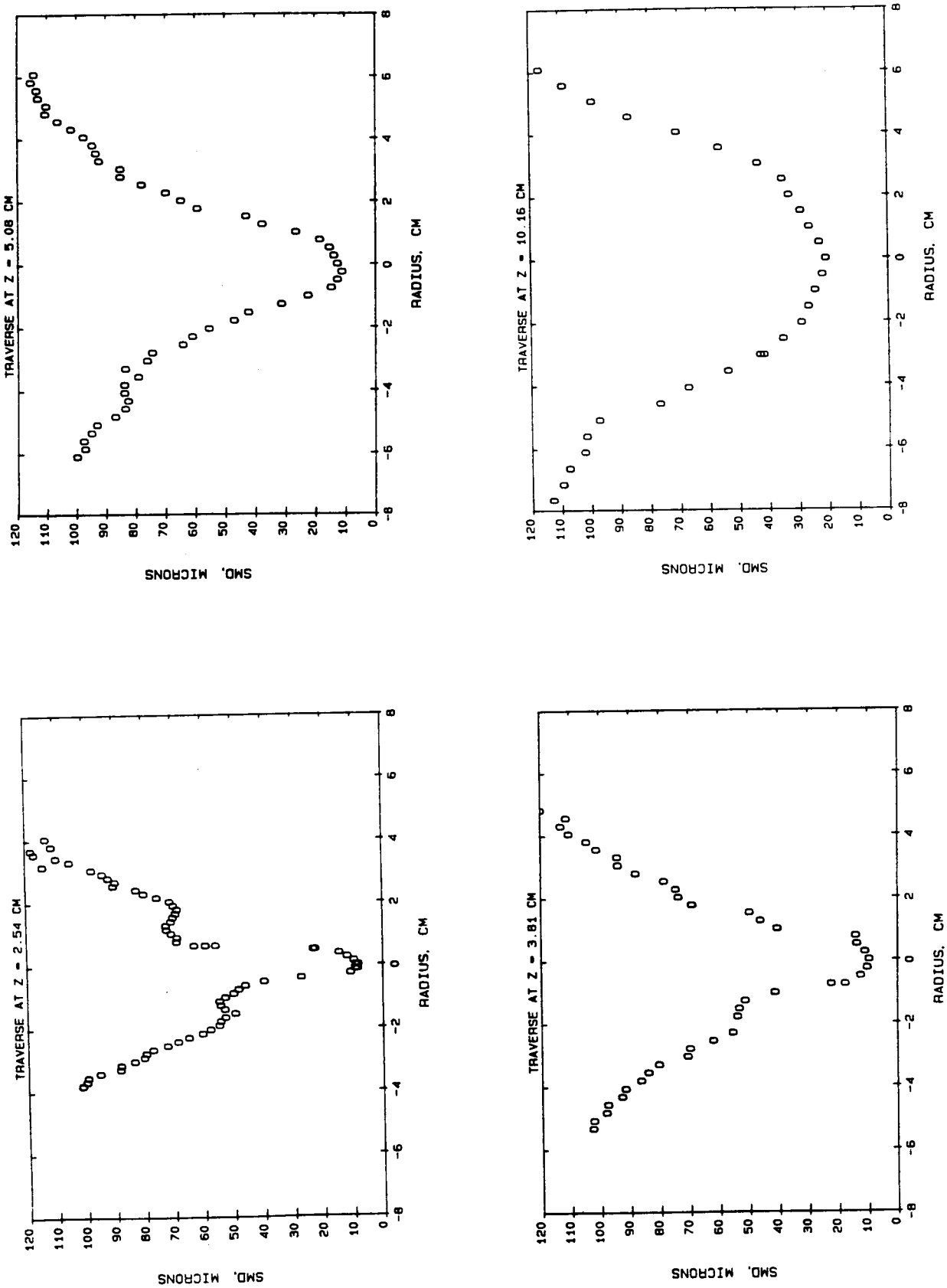

Figure 27. Droplet size distribution.

87-10-66-25

In general, very high radial gradients in SMD exist at all measurement locations.

The irregularities in the data patterns, particularly noticeable at the most upstream station result from clipping the droplet size distribution due to the inability of the PDA instrument to process all sizes and velocities of droplets with one processor setting. (As noted before, "file-splicing" techniques are available for handling this problem; however, they were not utilized in this study.) The clipping was encountered only at a few measurement stations in regions where both high radial velocity and SMD gradients were present.

Inspection of the data also shows that values of SMD measured at the positive radii are higher than those measured at negative radii. The discrepancy is most notable at the edges of the spray at the upstream region where the droplet number densities are highest. Based on discussions with the instrument developer, this discrepancy is probably associated with interference of the transmitted beams which form the probe volume by the dense spray rather than with interference of the scattered light captured by the receiving optics. The values measured at negative values of radius should therefore be more accurate.

Volume Flux

The PDA instrument can be used to measure the mass (volume) flux distribution in cases where an accurate count of signal rejections can be made (few instances of multiple particles in the sampling volume) and where the flow is nearly undirectional. These benign conditions certainly do not exist in this flow and therefore only the qualitative nature of the results (Fig. 28) is significant. The hollow cone nature of the spray is made evident by the depression of the centerline values and by the profile spreading with increasing downstream distance. The fact that the measurements are not quantitatively accurate is evident by an increase in the peak concentration values with increasing axial distance, rather than a decrease. Also, integration of the measured volume-flux distribution at the most downstream station yields a total flow rate of 500 kg/hr--far in excess of the metered value of 71 kg/hr. According to the instrument developer, this error in measuring the volume flux is associated with the techniques employed in estimating the size of the probe volume. This estimate is based on a statistical analysis of the number of fringe crossings detected during the sampling period; a biased result is obtained in flows where there is a significant component of particle velocity in the plane of the fringes. Improved quantitative measurements of mass flux in high-velocity, swirling flows will require the use of higher-speed processors and a multi-velocity-component system.

A comparison of the mass flux measurements acquired by the PDA instrument with that acquired by the patternator is shown in Fig. 29. The data have been normalized by the peak-value in each data set. Based on extensive experience with the patternator and the fact that the metered and integrated flow rates are in close agreement, it is believed that the patternator data are quite accurate. The probe array is intrusive, however, and may influence the flow--particularly the swirl component of velocity which must accommodate to the walls of the probe array downstream of the measurement station. The mean radius of the spray as measured by the PDA instrument is seen to be

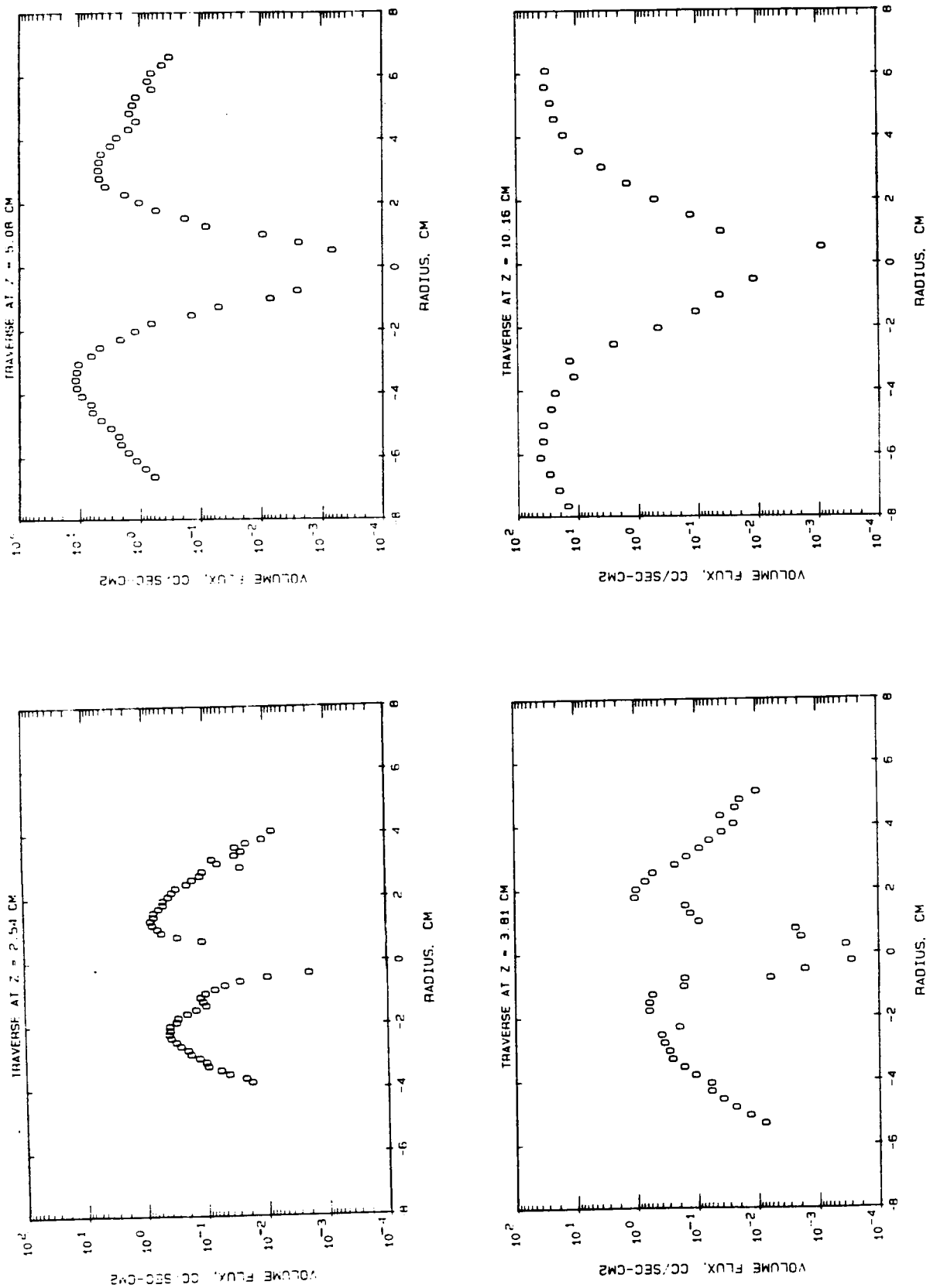

Figure 28. Volume flux distribution.

87-10-66-26

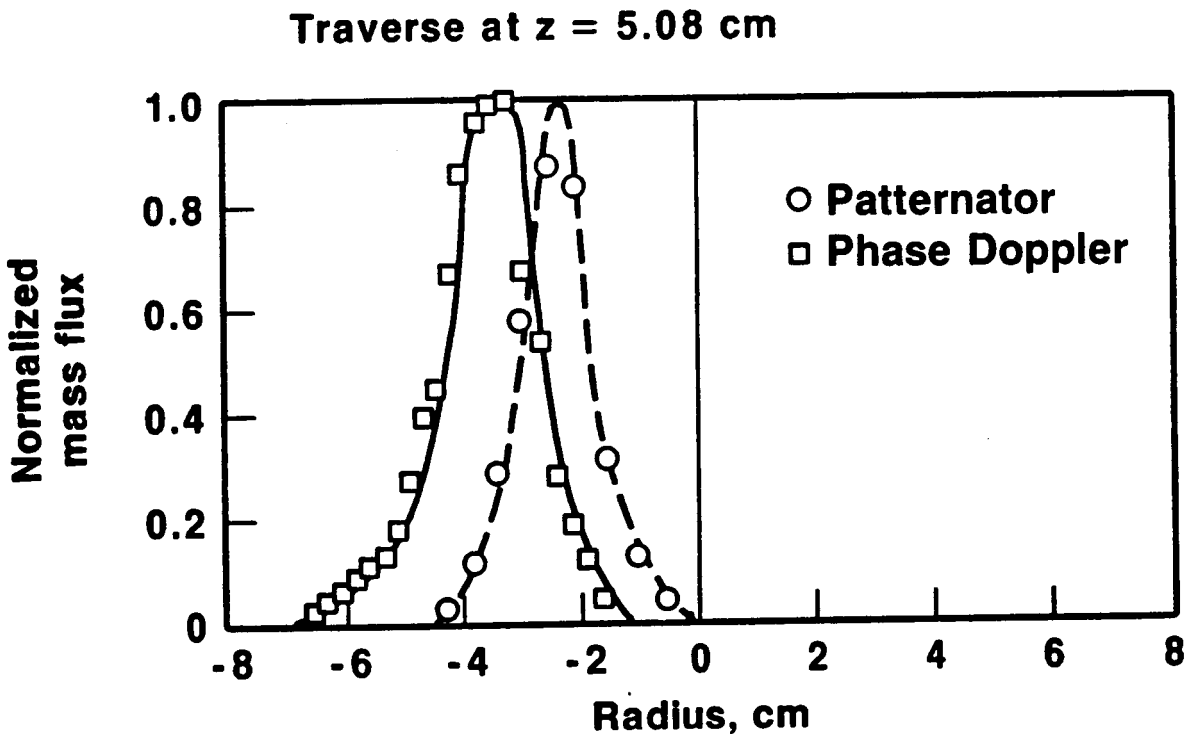

Figure 29. Mass flux measurement comparison.

87-10-66-21

significantly larger than that measured by the patternator. The measured thickness of the spray sheet is somewhat larger in the case of the PDA. Until more accurate PDA data are available, either through testing at reduced flow conditions or through instrumentation improvements, it must be assumed that the patternator provides a more accurate representation of the spray.

CONCLUDING REMARKS

Instrumentation techniques currently available are capable of providing significant information on the behavior of airblast injectors operating under high flow conditions - flow rates on the order of 70 kg/hr and velocities on the order of 125 m/sec. Mass flux, droplet size distribution, and flow velocity data have been acquired.

The data obtained in this study provide information that can be used in the evaluation of analytical models. The velocity information possesses significant structure (variation as a function of radius) which undergoes substantial change from measurement station to measurement station. As a result, a useful modeling test can be based on this information.

The SMD data, while possessing a significant structure, does not undergo such a dramatic change with measurement station location. The most significant change in SMD distribution occurs in the region upstream of the first measurement station--a region too dense for accurate measurements with current instrumentation.

The mass-flux distribution produced by the patternator also shows significant structure. Probe interference effects may bias the patternator information, but to date, optical (nonintrusive) data do not exist which are known to be of superior quality.

Fluid mechanic analysis of the flow studied herein will establish whether the range of measurements conducted is sufficient to judge the adequacy of different analytical treatments. It is recognized that certain information required for analysis is lacking, in particular, the initial droplet size distribution. As a result, it will be necessary to evaluate the effect of assumed initial droplet distributions in a parametric manner. From the point of view of developing a practical design procedure, it would be of value to use existing droplet size distribution functions and correlations found in the literature (Ref. 24) to establish the initial conditions. On the other hand, a best guess regarding an appropriate size distribution is afforded by consideration of the reported PDA mass flux, SMD and velocity information at a given measurement station. (The assumptions inherent in using such an approach are: the relative mass-flux values are accurate; and vaporization, secondary atomization, and coalescence are negligible.)

It was recognized at the outset of this effort that use of a confined flow and the simulation of the spray by use of spherical particles of known size would eliminate substantial analytical difficulties. The experimental difficulties in performing extensive optical measurements through curved surfaces and preparing and injecting large quantities of microspheres made such an approach impractical for this program. Attempts to compare the results of these experiments with CFD predictions will be useful to direct the course of future efforts. Most significantly, such attempts will help to establish the level of accuracy which current analyses provide in predicting the spray character within a combustion chamber.

APPENDIX

Typical Phase-Doppler Anemometer PDF's

Plots showing particle diameter PDF's, velocity PDF's and size-velocity histograms are given in the following pages. Each page gives data obtained for a traverse at a specified plane downstream of the nozzle discharge plane. Data obtained at selected radii are given.

Each data subset shows the velocity range and size range for which data were collected. The PDF data show the normalized (relative to the maximum) bin count data. In the case of the droplet diameter data, the total (filled plus unfilled) bar height, which incorporates corrections for probe volume, is the preferred representation of the PDF.

The size-velocity correlations reflect the relative number of data realizations each size velocity class by the density of the pointed dots. Also, a line showing the mean velocity as a function of size is contained in size-velocity correlation plots.

TRAVERSE AT Z = 3.81 CM

R = 5.08

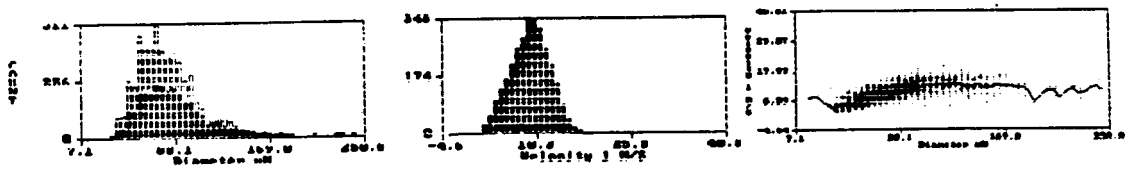

R = -2.29

R = -1.52

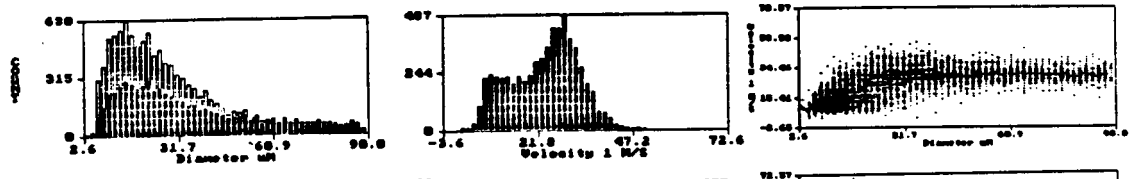

R = -1.02

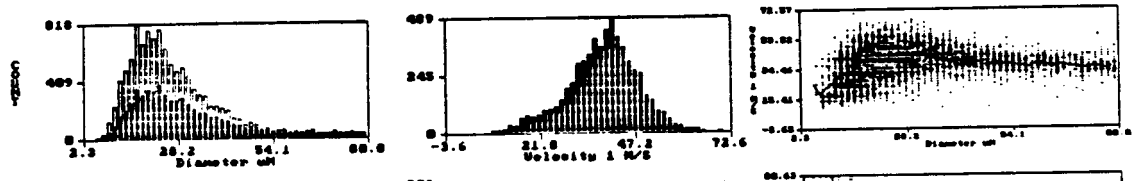

R = -0.508

R = 0

R = .508

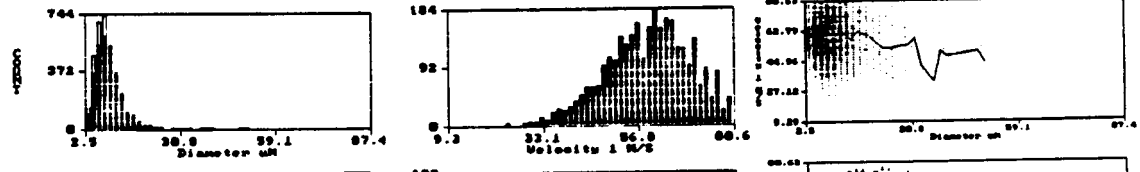

R = 1.02

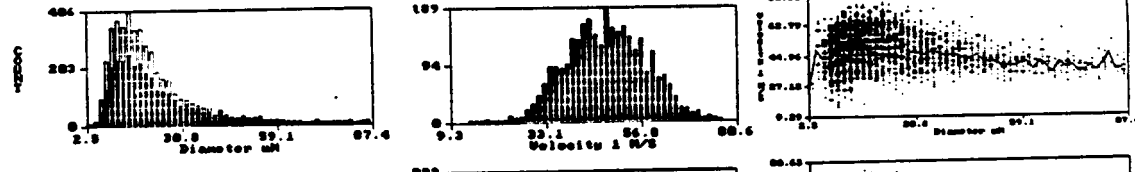

R = 1.52

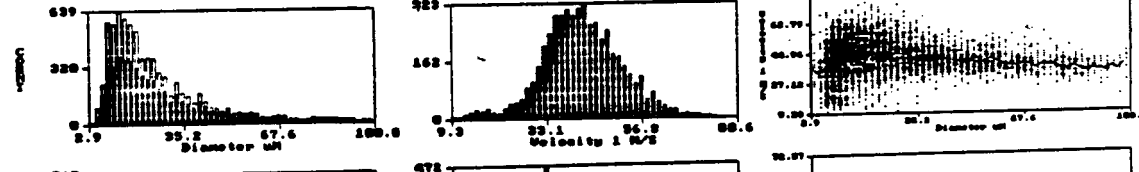

R = 2.29

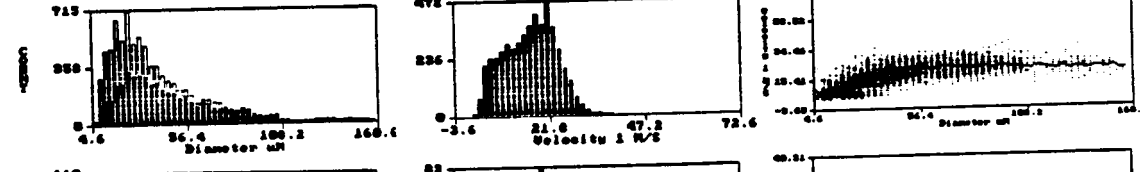

R = 5.08

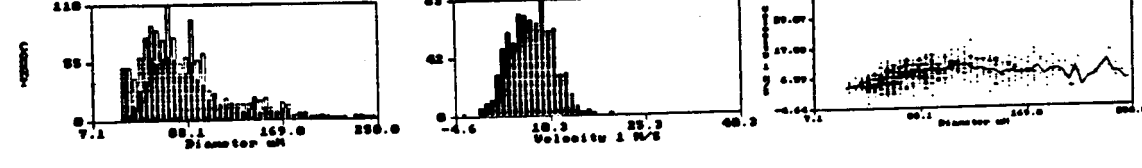

ORIGINAL PAGE IS
OE POOR QUALITY

TRAVERSE AT Z = 5.08 CM

R = -6.35

R = -3.81

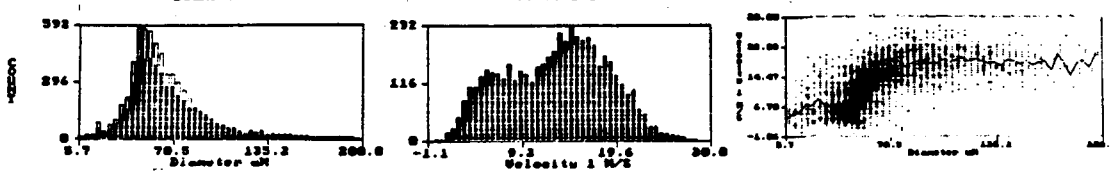

R = -2.29

R = -1.52

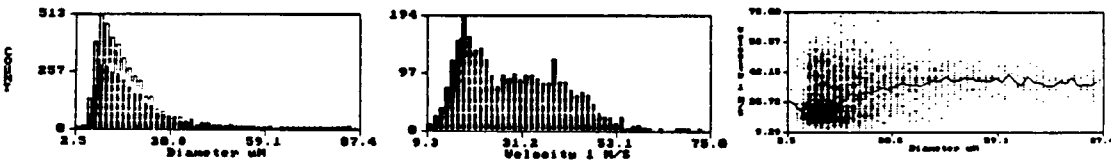

R = -.76

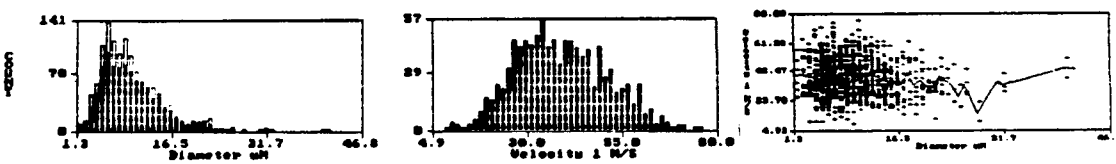

R = 0

R = 0.76

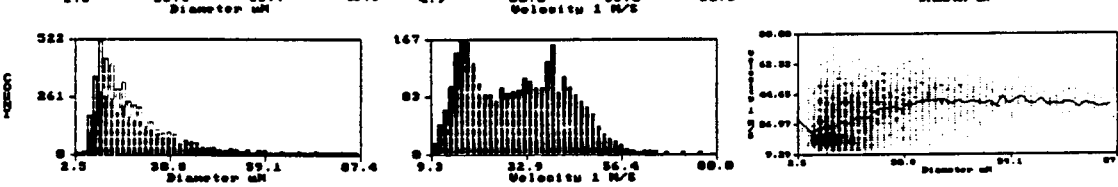

R = 1.52

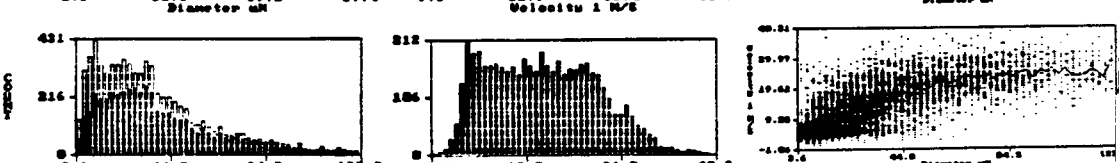

R = 2.29

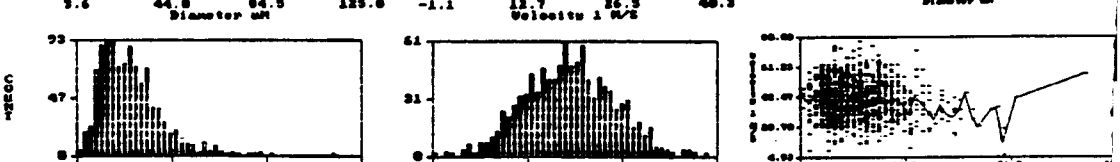

R = 3.81

R = 6.35

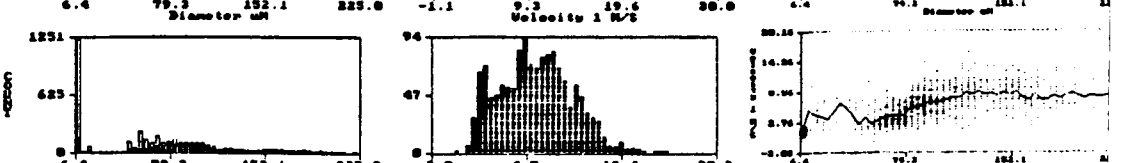

ORIGINAL PAGE IS
OF POOR QUALITY

TRAVERSE AT Z = 10.16 CM

R = -6.10

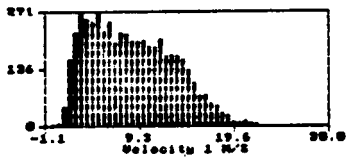

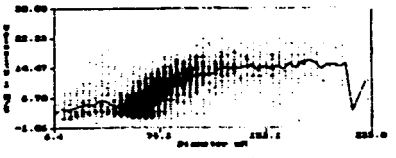

R = -4.57

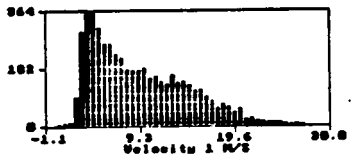

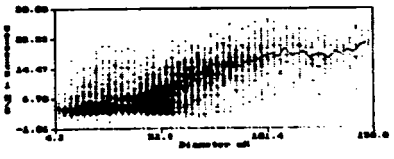

R = -3.05

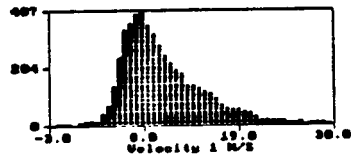

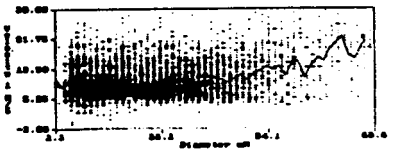

R = -2.03

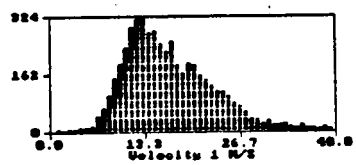

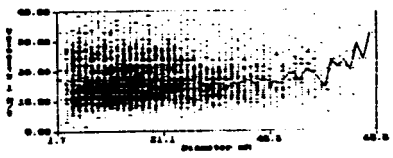

R = 1.02

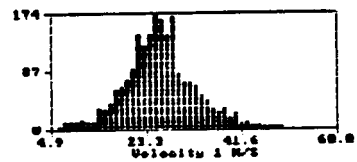

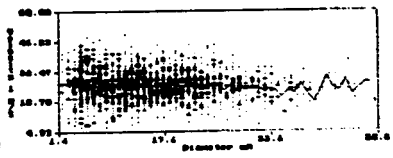

R = 0

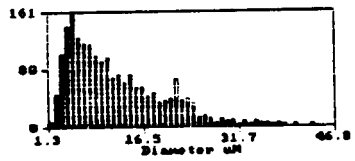

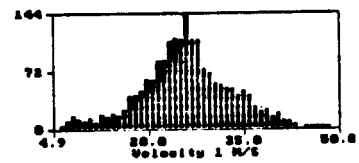

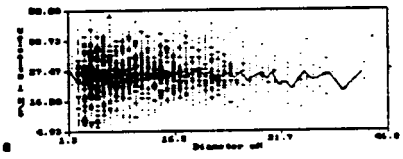

R = 1.02

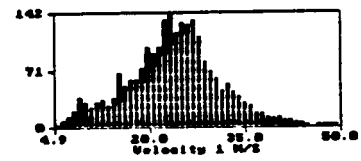

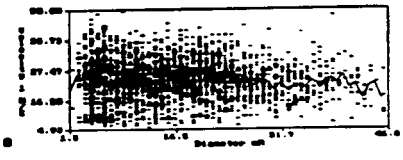

R = 2.03

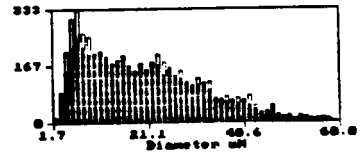

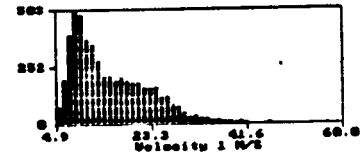

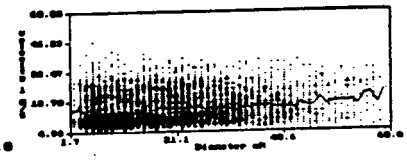

R = 3.05

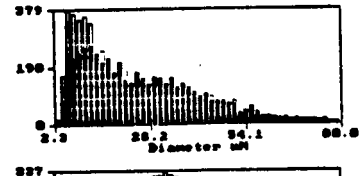

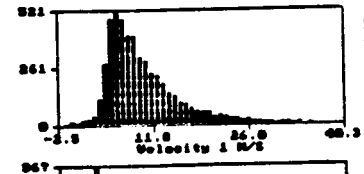

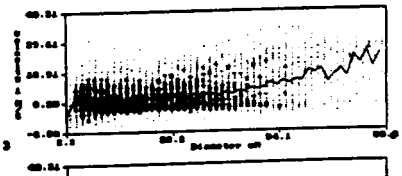

R = 4.57

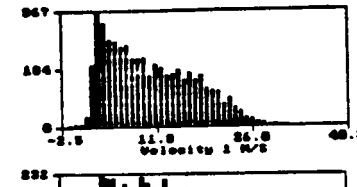

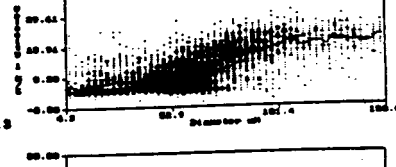

R = 6.10

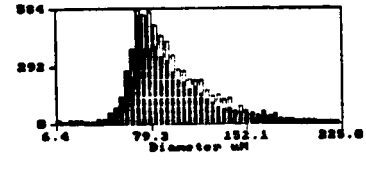

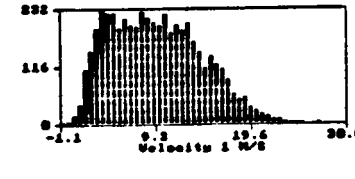

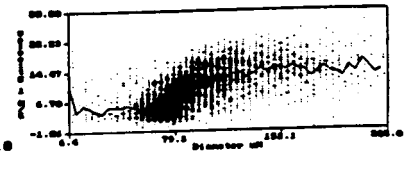

REFERENCES

1. Modarress, D., J. Wuerer and S. Elghobashi: An Experimental Study of a Turbulent Round Two-Phase Jet, AIAA Paper 82-0964, 1982.

2. Modarress, D., H. Tan, and S. Elghobashi: Two-Component LDA Measurement in a Two-Phase Turbulent Jet, AIAA-83-0052, 1983.

3. Modarress and H. Tan: LDA Signal Discrimination in Two-Phase Flows, Experiments in Fluids, Vol. 1, pp 129-134, 1983.

4. Shuen, J. S., A. S. P. Solomon, Q-F Zhang, and G. M. Faeth: A Theoretical and Experimental Study of Turbulent Particle-Laden Jets, NASA Contractor Report 168293, 1983.

5. Shuen, J. S., A. S. P. Solomon, Q-F Zhang, and G. M. Faeth: Structure of Particle-Laden Jets: Measurements and Predictions, AIAA Paper 84-0038, 1984.

6. Mostafa, A. A., H. C. Mongia, V. G. McDonell and G. S. Samuelsen: On the Evaluation of Particle-Laden Jet Flows: A Theoretical and Experimental Study, AIAA Paper 87-2181, 1987.

7. Bulzan, D. L., J-S. Shuen, and G. M. Faeth: Particle-Laden Swirling Free Jets: Measurements and Predictions, AIAA Paper 87-0303, January 1987.

8. Solomon, A. S. P., J-S. Shuen, Q-F Zhang and G. M. Faeth: A Theoretical and Experimental Study of Turbulent Nonevaporating Sprays, NASA Contractor Report 174688, June 1984.

9. Solomon, A. S. P., J-Shuen, Q-F Zhang, and G. M. Faeth: Measurements and Predictions for Nonevaporating Sprays in a Quiescent Environment, AIAA Paper 83-0151, January 1983.

10. Solomon, A. S. P., J. Shuen, Q-F Zhang and G. M. Faeth: Structure of Nonevaporating Sprays: Measurement and Predictions, AIAA Paper 84-015, January 1984.

11. Bachalo, W. E., M. J. Houser, and J. N. Smith: Behavior of Sprays produced by Pressure Atomizers as Measured Using a Phase/Doppler Instrument, Atomization and Spray Technology, Vol. 3, pp 53-72, 1987.

12. Rudoff, R. C., M. J. Houser, and W. D. Bachalo: Two-Phase Flow Measurements of a Spray in Turbulent Flow", AIAA Paper 87-0062, January 1987.

13. Kraemer, G., and W. Bachalo: Evaluation of a Phase Doppler Particle Analyzer for Measuring Dense Sprays from a Gas Turbine Fuel Injector, AIAA 86-1532, June 1986.

14. Jackson, T. A. and G. S. Samuelsen: Spatially Resolved Droplet Size Measurements, ASME 85-GT-38, March 1985.

15. McDonnell, V. G., C. D. Cameron and G. S. Samuelsen: Symmetry Assessment of a Gas Turbine Air-Blast Atomizer, AIAA Paper 87-2136, 1987.

16. McDonnell, V. G., C. P Wood, and G. S. Samuelsen: A Comparison of Spatially-Resolved Drop Size and Drop Velocity Measurements in an Isothermal Chamber and a Swirl-Stabilized Combustor, 21st Symposium (International) on Combustion, 1986.

17. Wang, G., C-P. Mao, J. Dietvorst, and N. Chigier: "An Experimental Investigation of Air-Assist Non-Swirl Stomizer Sprays, Atomization and Spray Technology, Vol. 3, pp 13-36, 1987.

18. Gosman, A. D., and E. Ioannedes: Aspects of Computer Simulation of Liquid-Fueled Combustors, Journal of Energy, Vol. 7, 1983, pp. 482-490.

19. Elgohbashi, S. T. Abou-Arab, M. Rizk, and A. Mostafa: Prediction of the Particle-Laden Jet with a Two-Equation Turbulence Model, Int. Journal of Multiphase Flow, Vol. 10, 1984,p p. 697-710.

20. Asheim, J. P., J. E. Kinwan, and J. E. Peters: Modeling of a Hollow-Cone Liquid Spray Including Droplet Collisions, AIAA 87-0135, 1987.

21. Ashgriz, N. and P. Givi: Coalescence Collision of Fuel Droplets, AIAA 87-0138, January 1987.

22. Soo, S. L.: Fluid Dynamics of Multiphase Systems, Blaesdell, Waltham, MA, 1967.

23. Faeth, G. M.: Evaporation and Combustion of Sprays, Progress in Energy Combustion Sciences, Vol. 9, 1983, pp. 1-76.

24. Lefebvre, A.: Gas Turbine Combustion, McGraw-Hill, New York, 1983, p. 413.

25. Rosfjord, T. J. and S. Russell: Influences of Fuel Spray Circumferential Uniformity, AIAA Paper 87-2135, July 1987.

26. McVey, J. B., S. Russell and J. B. Kennedy: "High-Resolution Patternator for the Characterization of Fuel Sprays, Journal of Propulsion, Vol. 3, 1987, pp. 202-209.

27. Swithenbank, J., J. M. Beer, D. S. Taylor, D. Abbot and G. C. McCreath: A Laser Diagnostic Techniques for the Measurement of Droplet and Particle Size Distribution, AIAA 76-69, January 1976.

28. Barth, H. G., ed: Modern Methods of Particle Size Analysis, Analytical Chemistry and Its Applications, Vol. 73, John Wiley & Sons, 1984.

29. Dodge, L. G.: Change of Calibration of Diffraction-Based Particle Sizes in Dense Sprays, Applied Optics, Vol. 23, 1984, pp. 626-630.

30. Craig, R. R., A. S. Nejad, E. Y. Hahn and K. G. Schwartzkopf: A General Approach for Obtaining Unbiased LDA Data in Highly Turbulent Non-Reacting and Reacting Flows, AIAA Paper 84-0366, January 1984.

31. Bachalo, W. D., C. F. Hess, and C. A. Hartwell: An Instrument for Spray Droplet Size and Velocity Measurements, ASME Paper 79-WA-GT-13, December 1979.

32. Bachalo, W. D. and M. J. Houser: Development of the Phase/Doppler Spray Analyzer for Liquid Drop Size and Velocity Characterizations, AIAA Paper 84-1199, June 1984.

33. Bachalo, W. D. and M. J. Houser: Optical Engineering, Vol. 23, 1984, p. 583.

34. Dodge, L. G.: Representation of Average Drop Sizes in Sprays, AIAA Paper 87-2133, 1987.

35. Garg, A. K. and S. Leibovich: Spectral Characteristics of Vortex Breakdown Flowfields, Physics of Fluids, Vol. 22, 1979, pp. 2053-2064.

36. Patrick, W. P.: Error Analysis for Benchmark Fluid Dynamic Experiments, UTRC Report R85-151772, June 1985.